UNCLASSIFIED

American Research Corporation of Virginia
P.O. Box 3406
Radford, Virginia 24143-3406

Laser Fiber Optic Sensor for Human Biomagnetic Measurements

Air Force SBIR Phase II Draft Technical Final Report
April 1990

R. J. Churchill, A. Sarrafzadeh, and H. P. Groger

Prepared for:

Armstrong Aerospace Medical Research Laboratory
Human Systems Division (AFSC)
United States Air Force
Wright-Patterson AFB, OH 45433-6573

Contractor: American Research Corporation of Virginia
Contract No.: F33615-87-C-0546

UNCLASSIFIED

UNCLASSIFIED
SECURITY CLASSIFICATION OF THIS PAGE

REPORT DOCUMENTATION PAGE

Form Approved
OMB No. 0704-0188
Exp. Date: Jun 30, 1986

1a. REPORT SECURITY CLASSIFICATION
Unclassified

1b. RESTRICTIVE MARKINGS

2a. SECURITY CLASSIFICATION AUTHORITY
N/A since Unclassified

3. DISTRIBUTION / AVAILABILITY OF REPORT
Not to be released outside the government for a period of two years without permission of contractor.

2b. DECLASSIFICATION / DOWNGRADING SCHEDULE
N/A since Unclassified

4. PERFORMING ORGANIZATION REPORT NUMBER(S)
ARC-TR-90-AFAAMRL-01

5. MONITORING ORGANIZATION REPORT NUMBER(S)

6a. NAME OF PERFORMING ORGANIZATION
American Research Corporation of Virginia

6b. OFFICE SYMBOL (If applicable)

7a. NAME OF MONITORING ORGANIZATION
Armstrong Aerospace Medical Research Laboratory

6c. ADDRESS (City, State, and ZIP Code)
P.O. Box 3406
Radford, Virginia 24143-3406

7b. ADDRESS (City, State, and ZIP Code)
Human Systems Division
Wright-Patterson AFB, OH 45433-6503

8a. NAME OF FUNDING / SPONSORING ORGANIZATION
Department of the Air Force
Air Force Systems Command

8b. OFFICE SYMBOL (If applicable)

9. PROCUREMENT INSTRUMENT IDENTIFICATION NUMBER
F33615-87-C-0546

8c. ADDRESS (City, State, and ZIP Code)
Department of the Air Force
Air Force Systems Command
Wright-Patterson AFB, OH 45433-6503

10. SOURCE OF FUNDING NUMBERS

PROGRAM ELEMENT NO.	PROJECT NO	TASK NO.	WORK UNIT ACCESSION NO.

11. TITLE (Include Security Classification)
Laser Fiber Optic Sensor for Human Biomagnetic Measurements

12. PERSONAL AUTHOR(S)
Russell J. Churchill, Adel Sarrafzadeh, and Howard P. Groger

13a. TYPE OF REPORT	13b. TIME COVERED	14. DATE OF REPORT (Year, Month, Day)	15. PAGE COUNT
Draft Final	FROM 880127 TO 900129	900412	77

16. SUPPLEMENTARY NOTATION

17. COSATI CODES		
FIELD	GROUP	SUB-GROUP

18. SUBJECT TERMS (Continue on reverse if necessary and identify by block number)
Laser, Fiber Optic, Interferometer, Magnetometer, Human Biomagnetism, Magnetostriction.

19. ABSTRACT (Continue on reverse if necessary and identify by block number)

The human body produces magnetic fields due to electric current sources generated by the muscles, nerves and other organs. The organs which produce the magnetic fields of interest in biomagnetism are the heart and the brain which generate fields around the chest and the head, respectively. Biomagnetic research has provided significant contributions to the study of magnetic activities in the human body. The presently available diagnostic tool for such applications (e.g. neuromagnetic fields as low as 10^{-14} Tesla) is the superconducting quantum interference device (SQUID) magnetometer. However, the SQUID sensor requires cryogenic instrumentation, thereby limiting the conditions under which the magnetometer can be used and contributing to a much high system cost. In order to permit the evaluation of human biomagnetic fields under mission operating conditions, this program involved the development of a compact, sensitive, room-temperature biomagnetic sensor based on a laser-stimulated fiber optic interferometer with magnetostrictive field sensing elements. The overall goal of the Phase II research program was to demonstrate the

20. DISTRIBUTION / AVAILABILITY OF ABSTRACT
☐ UNCLASSIFIED/UNLIMITED ☒ SAME AS RPT. ☐ DTIC USERS

21. ABSTRACT SECURITY CLASSIFICATION
Unclassified

22a. NAME OF RESPONSIBLE INDIVIDUAL
Dr. Glenn F. Wilson

22b. TELEPHONE (Include Area Code)
(513) 255-8748

22c. OFFICE SYMBOL
AAMRL/HEG

DD FORM 1473, 84 MAR

83 APR edition may be used until exhausted.
All other editions are obsolete.

SECURITY CLASSIFICATION OF THIS PAGE
UNCLASSIFIED

19. ABSTRACT continued

performance of fiber optic-based magnetic sensors to be used in human magnetocardiography (MCG) and magnetoencephalography (MEG). Previous work suggested the use of compact magnetostrictive transducer elements combined with fiber optic interferometric sensing for noncontact, room temperature and non-invasive detection of extremely weak biomagnetic fields. Such a sensing system would bypass the use of superconducting quantum interference device (SQUID) magnetometers, which require cryogenic cooling. The emerging technology in this lightwave-based instrumentation is the combination of fiber optic sensing with specially designed compact sensor heads to develop a research tool that relates sensor output to biomagnetic excitation input signals in terms of the optical and magnetostrictive properties of the sensor materials. Such sensor system could find broad application in physiological monitoring of Air Force pilots during flight conditions as well as in medical research laboratories for clinical cardiology, neurology, biomechanics and robotics. The Phase II project dealt with construction and testing of several compact magnetometers for eventual medical and aerospace applications. Major research areas investigated during the previous reporting periods include computer modeling of human magnetocardiographic and magnetoencephalographic fields evaluation of active homodyne laser interferometers in the proposed fiber optic magnetometers, and experimental demonstration of several compact fiber optic magnetometers in simulated magnetocardiology (MCG) and magnetoencephalography (MEG) within an instrumented prosthetic manikin. The Phase II research effort constituted the investigation of the following technical objectives: extension of magnetostrictive/fiber interaction models; improvement of the fiber optic interferometer design; evaluation of methods to increase the magnetostriction-to-fiber strain transfer efficiency; integration of hybrid micro-optoelectronic magnetometers; application of multiple layer sensor arrays and gradiometer operation; acquisition of families of simulated biomagnetic test data and optimization of a proof-of-concept system. The prototype instruments described in detail in this technical report has the desired performance needed to make MCG measurements. Specifically simulated biomagnetic field measurements have resulted in minimum detectable magnetic fields of about 10 picoTesla. Alternative designs of gradiometers such as first-order and second-order configurations have been incorporated. Phase II research in developing interferometric fiber optic magnetometers has provided encouraging results concerning the application of such noncontacting techniques for biomagnetic measurements including magnetophysiology and/or neuro-cardiac diseases diagnostics. Considerable effort has already been made in demonstrating the performance characteristics of the prototype magnetometers. Simulation measurements were obtained in both the laboratory and the medical research facilities. It is expected that advanced system development of the sensor to be achieved in Phase III program will make it a rugged field usable instrument. Such a complete system will contain a series of multiple channel sensors for precise dipole localization and mapping purposes. The additional optimization in the interferometric magnetometer configuration should improve the magnetic field detection sensitivity so that the very weak brain signals can readily be recorded. The Air Force should benefit from a small biomagnetic sensor that permits continuous monitoring of the physiological conditions of flight personnel such as fighter pilots during combat flight and high-g maneuvers. The real-time MCG/MEG measurements may provide the precursor signals due to the unconsciousness and indicate the pilot workload, overload, stress and blackout. The miniaturized sensor heads would be embedded into a flight helmet or vest and be used in normal cockpit environments. ARCOVA is aggressively pursuing the future market and extension of the present technology for both the military and civilian applications.

TABLE OF CONTENTS

Abstract....ii

List of Figures....v

List of Tables....vi

List of Abbreviations and Symbols....vii

I. Introduction....1

II. Human Magnetism....3

III. Magnetic Field Sensing Devices....5

IV. Phase II Technical Objectives....14

V. Research Program....17

1. Extension of Magnetostrictive Material/Optical Fiber Interaction Theory and Computer Modeling....17
2. Improvement of Fiber Optic Interferometer Designs....18
3. Methods to Increase Magnetostrictive Strain Transfer Efficiency....20
4. Integrated Optoelectronic Magnetometers....20
5. Application of Sensor Array and Gradiometer....21
6. Acquisition of Families of Test Data....22
7. Optimization of Proof-of-Concept System....25

VI. Results and Discussion....27

1. Fiber Optic Interferometric Magnetic Field Sensor and Biomagnetic Computer Modeling....27
2. Improvement of the Fiber Optic Interferometers....29
3. Methods of Fabrication of the Sensor Heads....32
4. Present Magnetometer Technology at ARCOVA....33
5. Special Sensor Head Configurations and Serial Array....35
6. Laboratory Simulated Biomagnetic Field Measurements....36
7. Proof-of-Concept Prototype System....38

VII. Conclusions and Potential Applications....60

1. Conclusions....60
2. Accomplishment of Phase II Objectives....60
3. Potential Commercial Applications....62

VIII. Acknowledgements and Dissemination....64

IX. References....65

LIST OF FIGURES

Figure 1. Basic Fiber Optic Interferometer 13

Figure 2. Interferometric Ouput as a Function of Optical Phase Shift 13

Figure 3. Magnetic Levels of Body and Background Magnetic Fields and Detection Range of Conventional Magnetometers. 26

Figure 4. Magnetic Field Isocontour Maps for Radial Components of Brain Dipole Source 40

Figure 5. Magnetic Field Isocontour Maps for Tangential Components of Brain Dipole Source 41

Figure 6. Magnetic Field Isocontour Maps for Radial Components of Heart Dipole Source 42

Figure 7. Magnetic Field Isocontour Maps for Tangential Components of Heart Dipole Source 43

Figure 8. Schematic Diagram of Compensator System 44

Figure 9. Schematic Illustration of Laboratory Constructed Metglas®/Optical Fiber Magnetic Field Sensor with Four-Layer Cylindrical Shell. 44

Figure 10. Optoelectronic Module Components of He-Ne Laser Magnetometer 46

Figure 11. Perspective Illustration of Components for Laser-Diode Compact Magnetometer 48

Figure 12. Subcompact Magnetometer 49

Figure 13. Experimental Arrangements Fiber Optic Magnetometer Subsystems. 50

Figure 14. Waveforms and Spectra for Heart Signals: a and b, Input; c and d, Output 51

Figure 15. Waveforms and Spectra for Repeated Heart Outputs 52

Figure 16. Waveforms and Spectra for Alpha Rhythm: a and b, Input; c and d, Output Signals 53

Figure 17. Waveforms and Spectra for Beta Rhythm:
a and b, Input; c and d, Output Signals....54

Figure 18. Waveforms and Spectra for Output Brain Waves
Using Lock-in Amplification Technique....55

Figure 19. Waveforms and Spectra for Magnetometer System Noise:
a and b, Differential Amplifier; c and d, Lock-in Amplifier....56

Figure 20. Contour Map of Measured and Specially Enhanced
Spectral Peaks for 3 x 3 Grid Points....58

Figure 21. Conceptual Design of Instrument for Human
Magneto-electrophysiological Measurements....59

LIST OF TABLES

Table I. He-Ne Laser Based Compact Magnetometer Components....45

Table II. Laser Diode Based Compact Magnetometer Components....47

Table III. Low Pass Filtering Operators for Each Point on 3 x 3 Grid....57

Table IV. Application of Digital Averaging Technique....57

LIST OF ABBREVIATIONS AND SYMBOLS

A	Ampere
AC	alternating current
A/D	Analog-to-digital
B	magnetic flux density
C	magnetostriction constant
cos	cosine
°C	degree Centrigrade
Cr	chromium
Cu	copper
dB	decibel
DC	direct current
DMS	diluted magnetic semiconductor
DY	disprosium
e	electron charge
E_a, E_m, E_e, E_f	Young's moduli
ECG	electrocardiogram
EEG	electroencephalogram
f	frequency
Fe-B-Si	iron-boron-silicon
G	Gauss
g	gravitational constant
H, hf(t)	magnetic field strengths
H_B	bias magnetic field
h_{cal}	calibration magnetic field
He-Ne	helium-neon
Hz	Hertz
I	optical interferometric intensity
IBM PC-AT	trade name
i_n	noise current
i_s	signal current
i(t)	current
k	wavenumber
K	degree Kelvin
L, l, l_a, l_m	lengths
m	meter
μH	microHenry
MCG	magnetocardiogram
MEG	magnetoencephalogram
METGLAS	trade name
MOSFET	metal-oxide-semiconductor-field-effect-transistor
MPG	magnetopneumogram
Mumetal	trade name
n	refractive index
Ni	nickel
Oe	Oersted
P	optical power
PIN	positive-intrinsic-negative
PQRST	cardiac tracing
PS-21	trade name
PVDF	polyvinylidene fluoride
Q	quadrature
rad	radian
R	number of fiber lines
RF	radio frequency
r.m.s.	root mean square
RTV	trade name
R_v	Verdet constant
S	signal intensity
S/N	signal-to-noise ratio
sin	sine
SQUID	superconducting quantum interference device
T	Tesla
Tb	terbium
V	voltage
V_1,V_2, V_A, V_B,V_{01},V_{02}, V_{03},V_o	voltages
V_t, V_m, V_e, V_f	Volumes
W	Watt
2605-S2	trade name

Conversions (SI to cgs)	Symbols		Factors
$1\ A/m = \frac{10^3}{4\pi}\ Oe$	α	responsitivity	$K = 10^3$
$1\ rad = \frac{2\pi}{360}\ degrees$	λ	wavelength	$M = 10^6$
$1\ T = 10^4\ G$	Δ	differential operator	$f = 10^{-15}$
	$\Delta\upsilon$	detection bandwidth	$p = 10^{-12}$
	$\Delta\phi$	optical phase shift	$n = 10^{-9}$
	η	bonding efficiency	$\mu = 10^{-6}$
	θ	Faraday rotation angle	$m = 10^{-3}$
	π	3.1415	
	ψ	Phase constant	

I. INTRODUCTION

The human body produces magnetic fields due to electric current sources generated by the muscles, nerves and other organs. The organs which produce the magnetic fields of interest in biomagnetism are the heart and the brain which generate fields around the chest and the head, respectively. Biomagnetic research has provided significant contributions to the study of magnetic activities in the human body. The presently available diagnostic tool for such applications (e.g. neuromagnetic fields as low as 10^{-14} Tesla) is the superconducting quantum interference device (SQUID) magnetometer. However, the SQUID sensor requires cryogenic instrumentation, thereby limiting the conditions under which the magnetometer can be used and contributing to a much high system cost. In order to permit the evaluation of human biomagnetic fields under mission operating conditions, this program involved the development of a compact, sensitive, room-temperature biomagnetic sensor based on a laser-stimulated fiber optic interferometer with magnetostrictive field sensing elements.

The target of opportunity in this research project has been the development of a compact, highly sensitive, room-temperature magnetic field sensor to compete with the SQUID sensor in a large number of applications where the SQUID sensor is presently used exclusively. The laser-stimulated fiber optic magnetic field sensor developed in this program can have sensitivities approaching those of the SQUID sensor, can operate at room temperature and can be reduced in size so that excellent spatial resolution of magnetic fields can be obtained. From a commercial viewpoint the fiber optic sensor can be produced at a fraction of the cost of the SQUID sensor and can be configured in geometrical arrays for multi-axis measurements. Such a fiber optic magnetic field sensor would find applications in research and in a broad range of hospitals and clinics as a result of lower cost and greater ease of stabilization and use. The desired operating characteristics of a biomagnetic sensing system are as follows:

- High detection sensitivity (10^{-14} Tesla) at very low frequencies of interest (DC-100 Hz),
- Output stability at both short-term and long-term detection,
- Low system noise level,
- Linearity of response and high dynamic range,
- High spatial resolution and multi-axis sensing,
- Compact, lightweight, noncontacting, room temperature and cost-effectiveness,
- Shielding against interfering environmental noise.

The Air Force should benefit from a biomagnetic sensor that permits continuous monitoring of the physiological condition of flight personnel such as fighter pilots during combat flight and high–g maneuvers. Such a sensor could measure the small magnetic fields generated by the brain, heart and eyes as indicators of pilot workload, overload, stress and blackout. Ideally, the magnetic sensor could be fitted into a flight helmet or a pilot jacket over the chest and be

operational in normal cockpit environments. Additional requirements for the sensor include signal stability for short and long term operations, radiation shielding, multi-axis spatial resolution of magnetic fields using an array of sensors. These magnetic sensors could have numerous civilian applications in hospitals and clinics to monitor the biomagnetic signals emanating from the human body. At present, however, biomagnetic sensors have limited practical application in field conditions.

The overall goal of the Phase II research program was to demonstrate the performance of fiber optic-based magnetic sensors to be used in human magnetocardiography (MCG) and magnetoencephalography (MEG). Previous work suggested the use of compact magnetostrictive transducer elements combined with fiber optic interferometric sensing for noncontact, room temperature and non-invasive detection of extremely weak biomagnetic fields. Such a sensing system would bypass the use of superconducting quantum interference device (SQUID) magnetometers, which require cryogenic cooling. The emerging technology in this lightwave-based instrumentation is the combination of fiber optic sensing with specially designed compact sensor heads to develop a research tool that relates sensor output to biomagnetic excitation input signals in terms of the optical and magnetostrictive properties of the sensor materials. Such sensor system could find broad application in physiological monitoring of Air Force pilots during flight conditions as well as in medical research laboratories for clinical cardiology, neurology, biomechanics and robotics.

During the first six-month period, January to July 1988, a series of theoretical and experimental subtasks was undertaken to provide the laboratory design of fiber optic magnetostrictive sensors for use in the interferometric instrument. During the second six-month period, July 1988 to January 1989, the research activities were associated with the analysis of improved fiber optic interferometric magnetometers and MCG/MEG instrument requirements for construction of a "table-top" experimental magnetometer system. During the third six-month period, January to July 1989, the work constituted the evaluation of the (helium-neon laser and laser-diode based) compact magnetometers for their laboratory performance. During the fourth six-month period, July 1989 to January 1990, the research areas included the acquisition of families of test data in simulated biomagnetic experiments and optimization of laboratory prototype devices. In addition, the performance capabilities of the Phase II program were demonstrated in front of a team of medical doctors at a medical research hospital (Charlotte Memorial Hospital and Medical Center, Electro-Physiology Laboratory).

This final report briefly reviews the work performed during the 24-month period incorporation progress on overall features and performance characteristics of the fiber optic magnetometer system. In addition, the report includes the recent findings and results on instrumented manikin biomagnetic test signals and presentation of computer techniques for the output signal response analysis, display and graphics.

II. HUMAN MAGNETISM

Biomagnetism refers to the study of magnetic fields originating in biological systems (WILLIAMSON and KAUFMAN, 1984). Three principal sources of biomagnetic fields have been identified: electric currents associated with the movement of ions, remanent magnetic moments of contaminants, and paramagnetic or diamagnetic constituents of the body when subjected to an applied magnetic field (ROMANI et al., 1982). Magnetic fields produced by electric currents have received the greatest attention. The pioneering experiment in this area was the detection of ion movements in the heart-muscle (BAULE and McFEE, 1963). In this study biomagnetic fields from the heart were observed using a pair of induction coils arranged in a gradiometer configuration placed over the chest. Later, COHEN et al. (1970), using a SQUID magnetometer and magnetic shielding, developed a magnetocardiograph (MCG) with quality comparable to that of the electrocardiograph (ECG).

All three sources of biomagnetic fields produce useful information on normal physiology and on abnormalities resulting from genetic disease or environmentally-induced illness. For example, measurable magnetic fields have been detected in the paramagnetic iron stored in the livers of patients having certain genetic diseases such as hemochromatosis or thalassemia. Remanent magnetic fields have been measured near the lungs of workers exposed to magnetic dust from such sources as the arc welding of steel. Other biomagnetic field detection milestones include monitoring such body parts as the abdomen (COHEN, 1969), skeletal muscles (COHEN and GIVLER, 1969), the fetal heart (HUKKINEN et al., 1976) the eyeball (KARP et al., 1976), the retina (AITTONIEMI et al., 1979), skeletal muscles and hair follicles (COHEN et al., 1980).

In addition to its relevance for clinical measurement, biomagnetism has important uses for the military. For instance, neuromagnetometry, measuring neuromagnetic fields, would be useful for monitoring fighter pilot brain activity and could detect blackouts during high-g maneuvers. A magnetoencephalogram (MEG), the magnetic counterpart of the electroencephalogram (EEG), records these neuromagnetic fields. However, the biomagnetic fields associated with neural activity are the weakest of all biomagnetic fields detected thus far. The flux density of brain magnetic fields is on the order of 10^{-13} to 10^{-12} Tesla (BEATTY et al., 1986). This is at least two orders of magnitude smaller than fields produced by skeletal muscles or the heart. Most biomagnetic experimental work carried out presently is achieved with the SQUID magnetometer, which is acceptable for clinical applications. However, SQUID systems require cryogenic cooling and are too large for many defense applications, thus necessitating the refinement of the fiber optic interferometric magnetometer.

The magnetic fields produced in the brain can be divided into two groups: steady-state fields arising from spontaneous brain activity, such as alpha rhythms or delta waves; and fields evoked by sensory stimuli, such as visual, auditory or

somatic stimuli. It is important to monitor these evoked fields because they provide information about neuronal activity that is different from information derived from evoked potentials measured at the skull (MIZUTANI and KURIKI, 1986). For example, there is a correlation between MEG and EEG signals of the alpha rhythms when the subject is awake, but this correlation is absent during sleep (WILLIAMSON and KAUFMAN, 1978). The study of brain activity evoked by sensory stimuli has been a productive area of neuromagnetic research. BRENNER et al. (1975) observed a somatically evoked field by applying a mild, repetitive, electrical stimulus to the little finger of the right hand and monitoring the changes in the emerging magnetic field over the left hemisphere of the brain. The center of the field pattern corresponds to the appropriate position on the sensory homunculus (WILLIAMSON and KAUFMAN, 1978). Similar experiments using visual stimuli, such as a repetitive bright flash of light, have been performed. BRENNER et al. (1975) found that the visually evoked field is sharply localized over the visual cortex. Auditory evoked fields have also been identified (SAMS et al., 1985).

Theoretically, biomagnetic fields emanating from a cortical source should and sometimes do approximate a dipolar field pattern (BEATTY et al., 1986). The magnetic flux emerges from one side of the magnetic source and re-enters the head on the other side of the source. However, such ideal field patterns are rarely seen in practice (BEATTY et al., 1986). Although clinical neuromagnetometry is still in its infancy, some interesting observations about neuromagnetic fields in individuals with abnormal brain activity have been made. COHEN (1972) reported abnormal brain activity in a single patient with psychomotor seizures, and HUGHES et al. (1977) used the MEG to study a number of neurological disorders, such as brain tumors, petit mal epilepsy and several psychiatric disorders accompanied by slow delta waves. More work is needed in the area of clinical neuromagnetism, even though the initial results have been promising.

Another biomagnetic field of interest to the military is produced by the heart. The measurement of these magnetic fields, whose magnitudes are on the order of 10 to 100 pico-Tesla, has been suggested for the diagnosis of cardiac disorders that affect cardiac activation such as conduction defects, infarction or arrythmias (WIKSWO et al., 1979). A comparison of magnetocardiography and electrocardiography has indicated that the magnetocardiograph data is more spatially specific than electrocardiograph data (MACAULAY et al., 1985) and could indicate functional abnormalities of the His-Purkinje system or the subendocardial activation of the left ventricular wall. The magnetocardiograph could be used to distinguish between benign and malignant T-wave abnormalities, identify the tissue areas responsible for generation of late potentials or evaluate ischemic and non-specific ST segment shifts. At present, the necessity of cryotechnology limits the application of magnetocardiography. It is believed that a fiber optic magnetometer for magnetocardiography will increase both the extent of this technique in practice as well as the resolution of magnetocardiography in identifying and diagnosing cardiac abnormalities.

III. MAGNETIC FIELD SENSING DEVICES

In this section an account is given of magnetic field sensors including induction coils, Hall effect magnetometers, magneto-optic devices, SQUID magnetometers, and interferometric fiber optic magnetometers. For purposes of comparison, the alternative measurement techniques are assessed for range of operation, sensitivity, susceptibility to noise and overall performance. This data is used for trade-off analysis with the fiber optic interferometric magnetometer.

Induction Coils

A search coil with a known number of turns and a known cross-sectional area can be used for measuring the flux density in a small region of a magnetic field. The device is connected to a ballistic galvanometer, called a fluxmeter. When the coil is quickly turned through a quarter turn or is moved from the field to a place where the flux density is zero, an electromotive force is induced whose magnitude is proportional to the rate of change of magnetic flux. If the instrument is properly calibrated through deflection of the galvanometer, the value of the flux density can be determined. The sensitivity of the fluxmeter depends upon the value of the flux density within the air gap of the galvanometer, so that the sensitivity increases for weaker fields in the gap. Typical sensitivities of fluxmeters range from 0.6×10^{-5} G (0.6×10^{-9} T) to 5×10^{-5} G (5×10^{-9} T). Since the maximum deflection is obtained when the coil is placed with its plane perpendicular to the magnetic field, both the magnitude and the direction of the field can be obtained by observing the readings with the plane of the coil in different orientations. Alternatively, a fluxgate magnetometer can be used; this produces an electrical signal whose magnitude and phase are proportional to the magnitude and direction of the external field acting along its axis.

Hall Effect Magnetometer

The Hall effect is the development of a transverse electric field in a current-carrying conductor placed in a magnetic field. Usually, the conductor is positioned so that the magnetic field is perpendicular to the direction of current flow and the electric field is perpendicular to both.

For a square semiconductor plate placed in a transverse magnetic field and a constant current passing through it, a voltage appears which is proportional to the flux density. This principle is used in the Hall effect gaussmeter. It consists of a thin piece of silicon or other semiconductor material (millimeter size) inserted between the poles of a magnet to measure the magnetic field strength. As the silicon transducer converts the magnetic flux density to a proportional voltage, all characteristic parameters of time-varying magnetic fields can be measured. The typical Hall effect measurement instrument could have a wide dynamic range and high accuracy of 300 mG (3×10^{-5} T).

Magneto-Optic Device: The Faraday Effect

The Faraday effect is based on the linear relationship between the Faraday rotation angle (θ) and the magnetic flux density (B) in Faraday elements such as quartz, special glass, ferrite and special semiconductors. A linearly polarized optical wave (or microwave) is incident upon the Faraday element, whose plane of polarization is subject to rotation in the presence of a magnetic field. The rotation angle, θ, experienced by the wave after propagation through an effective length, L, of the sensor is related to the magnetic flux density as follows: $\theta = R_V LB$, where R_V is the Verdet constant, a measure indicating the size of Faraday effect of the sensor. The angle, θ, can be measured by an analyzer, polarimeter and interferometric ellipsometer.

Sensitivity depends on the polarimeter as well as the Verdet constant and the effective length of the Faraday element. A conventional differential polarimeter has been used to measure an angle as small as 0.1 milli-rad. Interferometric ellipsometers can measure θ's much smaller than conventional polarimeters. The highest Verdet constant reported is 0.17 degree/cm-G for diluted magnetic semiconductor (DMS) crystals. Therefore the sensitivity is 17 mG (17×10^{-7} T) with a 1cm DMS crystal in a double pass configuration (so that L = 2 cm) using a conventional polarimeter. The sensitivity should be better than 1.7×10^{-3} G (1.7×10^{-7} T) if an interferometric polarimeter is used.

The essential components of the magneto-optic system would include a Faraday element, a laser source and polarimeter consisting of a 20° Wollaston prism, two photodiodes with amplifiers, and a differential preamplifier (type-W) to use with a general purpose oscilloscope. When fiber optics are used for laser beam delivery, an additional directional coupler, three objective lenses and holders, and a polarization conserving optical fiber is needed.

SQUID Magnetometer

The unique properties of superconductors have led to the development of tiny measuring and computing devices, called SQUID (superconducting quantum interference devices). Most of these devices involve Josephson tunneling and operate at or below 4.2 K, the temperature of liquid helium. The major applications of SQUID are in magnetometers, computers, physical measurement standards and detectors of high-frequency electromagnetic radiation. Applications of SQUID magnetometers include low temperature research, geophysical measurements and the measurement of magnetic signals produced by the human heart and brain. A second derivative magnetic field gradiometer is used for medical measurements.

A SQUID magnetometer system was first used by COHEN et al. (1970) to detect the human magnetocardiogram and since that time has become the principal tool in biomagnetic measurements. There are two types of SQUID magnetometers for detecting magnetic flux: DC–SQUID and RF–SQUID which operate with a DC bias current and an RF bias current, respectively. In the conventional SQUID arrangement, the field of interest is sensed with a detection coil located inside the wall of the dewar. A detection coil, wound with superconducting wire, is led into the SQUID enclosure where it is connected to a superconducting input coil in close proximity to the SQUID. The biomagnetic field causes a current to flow in the detection coil. As this current passes through the input coil it imposes a magnetic field on the SQUID. The SQUID responds to this field and the response is measured by a sensitive preamplifier.

Biomagnetic measurements are usually made with an RF SQUID detector, consisting of a superconducting ring interrupted by a weak link which reduces the strength of the circulating current for a given applied magnetic field. The amplitude of the resultant RF voltage across the weak link is monitored and is found to vary periodically as a function of the externally applied magnetic field. Through an elaborate stabilization process, the values of the applied biomagnetic field may be determined.

Most SQUID sensors are used in conjunction with voltmeter circuitry, the sensitivity of which is typically 10^{-15} to 10^{-12} V/$\sqrt{\text{Hz}}$. A gradient SQUID is a magnetic field gradiometer in which two balanced superconducting pick-up loops are connected in series with a superconducting coil coupled to the SQUID. If a uniform magnetic field is applied, no flux is linked to the SQUID. The application of a field gradient, however, induces a flux in the SQUID proportional to the differences of flux between the two loops. Typical sensitivities are approximately 10^{-13}T m^{-1}/$\sqrt{\text{Hz}}$. A gradiometer can be adapted to measure the paramagnetic susceptibility of small specimens. A sample is inserted into one of the loops in the presence of a constant magnetic field, and the resulting change in flux is measured. A magnetometer system with a single pick up loop has a typical sensitivity of 10^{-14} T/$\sqrt{\text{Hz}}$.

Interferometric Fiber Optic Magnetometer

An interferometric fiber optic magnetometer is an optical phase sensor based on the two-beam Mach-Zehnder optical fiber interferometer. The magnetometer measures magnetic field amplitude through the interaction between magnetostrictive materials and optical fibers in the sensing element in one arm of the interferometer. Since the study of this magnetic sensor is the subject of research proposed under this project, the theoretical evaluation of the performance characteristics of a prototype system is detailed in the following paragraphs. Specifically, the paragraphs describe the efforts to tailor fiber optic sensor technology

to magnetostrictive transducers for the development of a prototype fiber optic magnetometer. The principle of operation and the effects of limiting factors on detection sensitivity of weak magnetic fields is investigated in this segment of the research.

The interferometric fiber optic sensor is one class of fiber optic sensors which use the inherent intrinsic or extrinsic sensing properties of flexible optical fibers. Since the optically stimulated sensor undergoes an optical phase shift caused by changes in the physical properties to be measured, a phase-tracking system can be used for the detection. However, optical frequencies are extremely high (~ 10^{15} Hz); as a result, phase-change monitoring at such high frequencies becomes impractical. This problem has been solved by converting the phase information into an intensity signal. Optical phase-modulation is typically achieved by two-beam interferometers. **Figure 1** shows a simple fiber optic interferometer of the Mach-Zehnder type, in which the phase shift of a coherent light passing through the sensing arm of the fiber is measured (with respect to the reference fiber) by the action of the fiber optic interferometric sensor.

A continuous-wave, single-frequency, low-power laser or a pigtailed diode laser can be used to stimulate the single-mode optical fibers. The fiber, into whose front-end surface the laser beam is directly launched, is divided into two arms by a single-mode, biconical, fused tapered coupler. The two fibers are then combined (by a second coupler) to superimpose the coherent optical wavefronts and provide the output optical intensity. Although the total optical intensity consists of constant and fluctuating components, it is the time-varying component of the intensity which contains the phase-shift information. The interferometric intensity is written as

$$I = P[1 + \cos(\Delta\phi + \psi)]$$

where ψ is the phase constant between the two fibers and the coefficient P is a function of optical power and the contrast of the interferometric pattern. **Figure 2** represents the cosine squared variation of the intensity versus the optical phase shift, $\Delta\phi$. The change in the phase is introduced by the physical parameter to be measured in the sensing arm of the fiber as opposed to the unperturbed reference fiber. The phase shift is related to the intrinsic change in physical properties of the optical waveguide, i.e.

$$\Delta\phi = \Delta(kl)$$

where $k = 2\pi n/l$ is the wave number in medium of the optical fiber, l is the fiber gauge length in the sensing arm, n is the refractive index of the fiber, and l is the optical wavelength. Thus,

$$\Delta\phi = \frac{2\pi}{\lambda}[(\Delta n)l + n\Delta l].$$

The first term in the bracket is usually small in comparison with the second, unless the refractive index is changed considerably because of a nonlinear effect caused by intense optical power. The change in axial length of the sensing fiber is the main contributor and is the linear transformer to the physical variable of interest. Therefore, the time varying intensity with respect to dynamic Δl can be written as

$$S = P \cos\left(\frac{2\pi n}{\lambda}\Delta l + \psi\right).$$

As was mentioned earlier, the change in optical fiber path length caused by the interrogating physical variable produces the output optical intensity which can directly be measured, once the relation between the variable and Δl is known. The transformation mechanism is the subject of the following section.

Interferometric Response vs. the Magnetic Sensing Transducer

The magnetic sensing element of the fiber optic system is the fiber which effectively converts the magnetostrictive perturbation of the sensor head material into optical phase changes of the laser beam propagating in the sensing fiber. The degree of strain in the optical fiber depends on the magnetoelastic deformation of the magnetostrictive materials and the bonding efficiency through which the mechanical deformation is transferred to the fiber material.

In amorphous metallic alloys, the mechanical strain in the direction of the magnetic easy-axis is a nonlinear function of the magnetization field (LIVINGSTON, 1982), i.e.

$$\frac{\Delta l_m}{l_m} = CH^2$$

where the left hand side is the strain or magnetostriction response, C is the material constant at saturation magnetization and the total magnetizing force upon the material is

$$H = H_B + H_{ambient.}$$

In general, the interferometric sensor can measure the AC field, the fluctuating $H_{ambient} = h\, f(t)$, but not the DC field, H_B. The presence of the static field in some cases can help to optimize the magnetostrictive response by directional aligning of the ferromagnetic domains. For the length, l_m, of magnetostrictive material parallel to the direction of the interrogating magnetic field,

$$l = Rhl_m$$

where R is the number of optical fiber lines bonded on l_m, and h is the fiber/material bonding coefficient. Therefore,

$$\Delta l \cong R\eta\, lm\, C\left[H_B^2 + 2\, H_B\, h\, f(t)\right]$$

where the second-order term in the dynamic field is neglected. Substituting the above into the signal information,

$$S = P\cos\left[\left(\frac{2\pi n}{\lambda}\, R\eta\, l_m C H_B^2 + \psi\right) + \frac{4\pi n}{\lambda} R\eta\, l_m C H_B\, h\, f(t)\right].$$

At the quadrature point, where the rate of change in optical signal intensity with respect to interferometric phase change is maximum, the first term in theargument of the cosine function should be

$$\frac{2\pi n}{\lambda} R\, \eta\, l_m\, C H_B^2 + \psi = \frac{2m+1}{2}\pi$$

where m is an integer. This is accomplished by introducing a phase shift to one arm of the fiber. This produces

$$S = P\sin\left[\frac{4\pi n}{\lambda} R\eta\, l_m C H_B\, h\, f(t)\right].$$

For small magnetic fluctuations,

$$\frac{4\pi n}{\lambda}\, R\, \eta\, l_m C H_B\, h f(t) \ll 1$$

and

$$\sin\left[\frac{4\pi n}{\lambda} R\eta\, l_m C H_B\, h\, f(t)\right] \cong \frac{4\pi n}{\lambda} R\eta\, l_m C H_B\, h\, f(t)\ .$$

hence,

$$S = \frac{4\pi n}{\lambda}\, PR\eta\, l_m C H_B\, h\, f(t).$$

That is, the output of the interferometer is linearly related to the magnitude of a time-varying magnetic field. The above relation is the basis for the absolute measurement of the small magnetic field magnitudes.

Magnetic Detection Sensitivity

The conventionally used photon-to-electron converter is a photodetector current with quantum efficiency of a (Amperes per Watt) as given by

$$i_s = \alpha S = \frac{4\pi n}{\lambda} PR\alpha\eta\ l_m C H_B\ h f(t).$$

The output current is converted into voltage output through the load resistance of the electronic signal analyzer. For calibration purposes, the maximum peak-to-peak voltage is first observed to determine the maximum phase shift of a full interferometric fringe cycle. The applied magnetic field is sufficiently large that

$$\sin\left[\frac{4\pi n}{\lambda} R\eta l_m C H_B h f(t)\right] = 1,$$

i.e.

$$\frac{4\pi n}{\lambda} R\eta\ l_m C H_B h f(t) = \pi/2.$$

Then, the calibrating magnetic field is determined by

$$h_{cal}\ f(t) = \frac{\lambda}{8\, n R\ \eta\ l_m C H_B}$$

For small magnetic field measurements, the optical shot-noise of the photodetector acts as a limiting mechanism for the detection. This fluctuating small current, in r.m.s., is represented as

$$i_n = (2e\alpha\ S\Delta\upsilon)^{1/2}$$

where e is the electron charge and Δu is the detection bandwidth. The minimum detectable magnetic field is determined for the signal-to-noise ratio of unity, i.e.

$$\frac{i_s}{i_n} = \frac{\alpha S}{(2e\ S\Delta\upsilon)^{1/2}} = 1$$

or

$$\frac{4\pi n}{\lambda} PR\alpha\eta l_m C H_B\ H_{min} f(t) = (2e \frac{4\pi n}{\lambda} PR\ \alpha\eta l_m C H_B\ H_{min} f(t)\ \Delta\upsilon)^{1/2}$$

Hence

$$H_{min}\, f(t) = \left(\frac{e \lambda \Delta \upsilon}{2\pi n P R \alpha \eta\, l_m C H_B} \right)$$

For example, let

$e = 1.6 \times 10^{-19}$ columb,
$l = 0.6\mu m$,
$\Delta\upsilon = 100$ Hz,
$n = 1.46$,
$P = 5\ \mu W$,
$R = 8$,
$\alpha = 0.3$ A/W,
$h = 50\%$,
$l_m = 0.125$m,
$C = 1.9 \times 10^{-9}\ (A/m)^{-2}$,
$H_B = 1.8$ A/m,

then

$H_{min} = 6 \times 10^{-12}$ Ampere/meter.

In addition to photodetection shot-noise, factors such as photoelectronic, thermal, and laser noises could practically limit a minimum field detectability. Thus, a higher H_{min} than calculated above is expected.

The previous Phase I research in developing interferometric fiber optic magnetometers has provided encouraging results concerning the feasibility of fiber optic magnetic field sensing techniques and has stimulated advanced research in optical sensor development for biomagnetic applications (CHURCHILL et al., 1987). The magnetic detecting element of such sensors consists of magnetostrictive materials mechanically coupled with one arm of an optical fiber Mach-Zehnder interferometer. The interferometer measures the phase shifts associated with fluctuating magnetic fields under interrogation. Although fiber optic sensing technology is being used increasingly to measure various physical properties, very low magnetic field sensing has not yet been fully developed. Research must identify practical ways to eliminate operational instabilities at very low frequencies and determine the most sensitive magnetostrictive materials to interact with the fiber sensor head. Once the optimal material is identified the magnetic sensitivity of interferometric fiber optic magnetometers can equal the high sensitivity of the SQUID magnetometers.

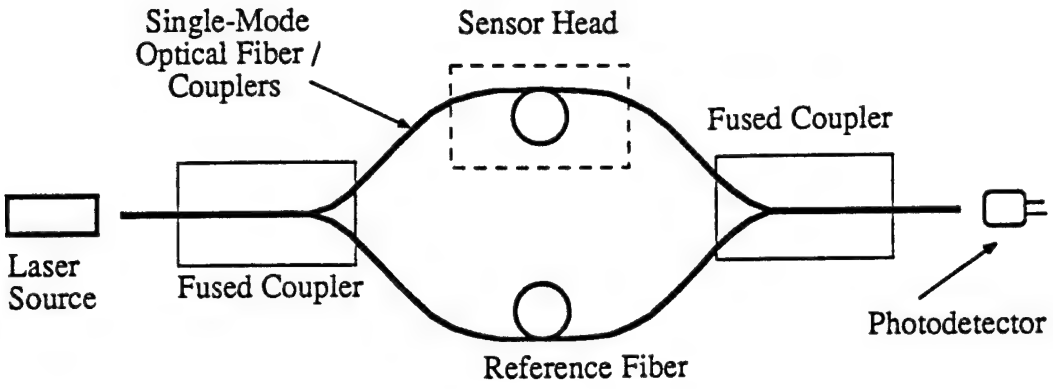

Figure 1. Basic Fiber Optic Interferometer.

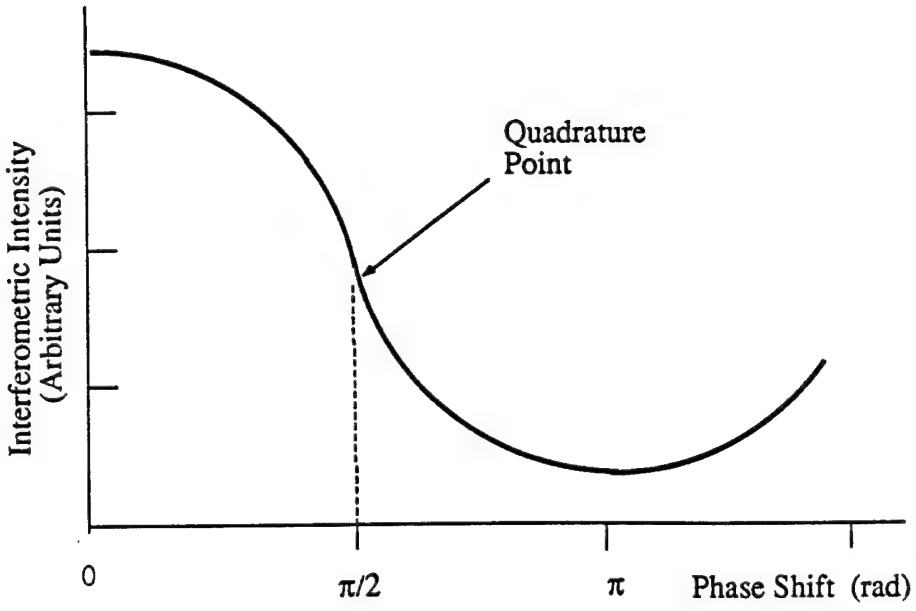

Figure 2. Interferometric Output as a Function of
Optical Phase Shift.

IV. PHASE II TECHNICAL OBJECTIVES

The Phase II Technical Objectives take into account the findings of the Phase I program and are directed toward research tasks leading to a prototype micro-optoelectronic magnetometer based on fiber optic interferometer sensing of magnetic fields emanating from organs of the human body. Specific objectives are as follows:

1. *To extend the theory and develop computer modeling techniques to assess the interaction between optical fibers and magnetostrictive materials in response to spatially distributed human magnetic fields having both radial and tangential components.*

The questions to be answered in this objective include the effects of spatial distribution of the magnetic fields on the magnetostrictive material geometry, the effects of temperature, background field, eddy current loss, response time and inherent magnetic properties of the material on the magnetostrictive response (strain), the effect of the epoxy adhesive and fiber coatings on the strain transfer mechanism, the effects of parametric changes of the optical fiber material on the strain-to-fiber optic path length conversion. A computer model is developed for the human biomagnetic measurement applications. The use of a coated optical fiber with an elastic coefficient matching that of the magnetostrictive materials and the use of bonded filaments of magnetostrictive material, can produce a sensor head with extremely long active sensing areas (long interaction lengths) without sacrificing flexibility. In order to optimize the choice of materials for the fiber magnetometer sensor head, and to specify the fiber spacings in integrated systems, it is necessary to model the magnetic and elastic system response under a variety of coupling conditions.

2. *To improve the existing interferometer design in order to achieve a desired phase shift sensitivity of better than 10^{-6} radian.*

This is accomplished by reducing unwanted optical fluctuations in the source and detector and by applying proper signal processing techniques for electronic noise reduction. In addition, the interferometric sensitivity is increased by means of more efficient methods of optical energy transfer, highly stable optoelectronic components, active homodyne signal nulling methods, and lock-in-amplification. An evaluation of the noise sources in the fiber interferometer system revealed that at low frequencies, laser noise determines the phase detection threshold of the interferometer system. Above 10 kHz, photodetector noise dominates the phase detection threshold. The optimal laser interferometer system would employ a low noise photodetector such as the Hamamatsu S1126 5BK and a frequency-stabilized laser such as the Coherent Model 200 or the Spectra Physics Model 117A.

3. *To evaluate experimental methods of increasing the efficiency of strain transfer from magnetostrictive materials to optical fibers in order to maximize the magnetic sensing response of the composite sensor heads.*

The investigation includes the use of polymeric and hybrid coatings as well as in-line/off-line bonding of magnetostrictive tapes onto the fiber-draw-processing and spooling. Questions to be investigated include the effectiveness of microbonding and graded coating techniques to enhance strain transfer and match the elastic properties of the hybrid components. The major factor affecting the sensitivity of the magnetometer is the value of the saturation magnetostriction measured as the fractional change in length of the material under a magnetic field. Once a magnetostrictive material is chosen, it must be bonded to the optical fiber in order to transfer strain developed as a result of the applied magnetic field. The Phase II program evaluates the effects of fiber coatings and the use of matched materials to improve strain transfer efficiency.

4. *To integrate the magnetometer device into a hybrid opto-electronic package consisting of source, detector and optical wave couplers in order to make a miniaturized field-usable sensor.*

The effects of degrading environmental parameters is studied, including vibration, acceleration and temperature. In addition the interaction of intense electro-magnetic and nuclear radiation with the fiber sensor components is studied. Questions of particular interest include packaging options to produce a compact, lightweight and rugged system as well as techniques to achieve low insertion losses, optimum intensity split, pigtailed coupling, switching and sensor multiplexing. This study considers the special configuration of multi-path fibers on the substrate including the use of micro-retroreflectors at the fiber ends and blazed grooved reflection etching on the terminal surfaces of the package.

5. *To develop magnetometer system components capable of operating in planar gradiometer and tandem probe configurations as well as of accepting data from multiple layer sensor arrays.*

This objective addresses questions of multiple layer integration and the reduction of background magnetic, thermal and electronic noise through active and passive shielding and compensation techniques. The approach to be taken includes developing a high resolution interferometer with electronic processing to reduce system noise, using annealed coated fibers, shielding system components from environmental noise, using rigid and planar circuitry to reduce vibration effects and employing second-order and third-order gradiometer systems.

6. *To acquire families of test data under laboratory and simulated clinical conditions for comparison with SQUID and other ultra-sensitive coil techniques.*

Questions on this objective relate to the quantification of magnetic field components and localized field perturbations derived from normal or abnormal conditions. Selected tests on simulated human subjects could be conducted using the magnetometer and SQUID sensor under screened room conditions in simulated laboratory environments at ARCOVA. Increasing interferometer phase sensitivity to 10^{-6} radian, developing signal processing, increasing fiber sensor length and optimizing strain transfer should extend system sensitivity to better than 10 pico-Tesla. This should lead to the successful demonstration of a fiber optic magnetocardiogram by the end of the Phase II program. Further improvements in system response should lead to the fabrication of a fiber magnetoencephalogram during the Phase III program.

7. *To optimize a proof-of-concept system and to assess the technical specifications for advanced engineering models of a fully-integrated interferometric fiber optic biomagnetic field sensor.*

The concept of a fully integrated system that incorporates multi-layered magnetostrictive material into the hybrid micro-optoelectronic package is developed. Questions to be considered include means of optically computing the signal for optimized performance, the use of scanning sensor arrays, probe design for specific brain/heart regions and fields, methods of short-term and long-term self-stabilization, susceptibility to damage, reliability, ultimate sensitivity, degree of nonintrusiveness and system cost-effectiveness. This objective investigates the design and development of specific sensor arrays and methods to achieve the signal processing requirements of the fiber magnetometer system.

V. RESEARCH PROGRAM

This section of the report describes the technical approach and the Phase II efforts relevant to the fiber optic biomagnetic field sensing research. Specifically, the program includes the approach taken for the completion of Phase II technical objectives; namely, extension of material/fiber interaction theory and biomagnetic computer modeling, improvement of fiber optic interferometer designs, evaluation of magnetic field sensing elements fabrication processes, integration of hybrid optoelectronic magnetometers, application of sensor array and gradiometer, acquisition of families of test data, and optimization of proof-of-concept system.

1. Extension of Magnetostrictive Material/Optical Fiber Interaction Theory and Computer Modeling

Technical Objective 1 requires an evaluation of the theory of strain transfer from the magnetostrictive sensor element to coated or uncoated optical fibers under the influence of biomagnetic fields. Magnetostriction is the change in dimension of a ferromagnetic material when it is placed along the axis of a magnetic field. The magnetostrictive effect has an important application in fiber optic- or piezoelectric-based magnetometers. The key element in a magnetostrictive fiber optic interferometric magnetometer is the sensor head which uses the combined effects of magnetostriction and optical phase shifting in the transducer elements. The magnetostrictive sensing element converts the magnetic field to be measured into a mechanical deformation. The single-mode optical fiber, mechanically coupled to the magnetostrictive material, converts the mechanical deformation, transferred through the bonded region, into an optical path length change. Thus, the fiber behaves as a strain gauge and as an intrinsic sensor. The change in the optical path length of the sensing fiber produces an optical phase shift in the optical field propagating in that arm. This phase-shifted optical field interferes with the unshifted field in the reference fiber arm. The optical intensity in the combined interferometer output is proportional to the applied magnetic field. Finally, a photodetector converts the output optical intensity into an electrical signal which can be digitized, amplified, filtered, displayed, stored and analyzed by electronic signal processing equipment.

For the composite magnetic sensor head using magnetostrictive amorphous metallic alloys, if the magnetostrictive material of volume V_m and elastic Young's modulus E_m (whose entire volume is subjected to the same field strength) is mechanically loaded with the epoxy adhesive and the jacketed optical fiber, the actual magnetostrictive response of the sensor head is less than the anticipated magnetostriction. According to the rule of mixtures, the expected magnetostrictive straining in the composite bonded sensor can be derived from

$$E_a V_t = E_m V_m + E_e V_e + E_f V_f$$

and

$$E_a \frac{\Delta l_a}{l_a} V_t = E_m \frac{\Delta l_m}{l_m} V_m$$

where $V_t = V_m + V_e + V_f$ is the total volume and E_a is the apparent Young's modulus of the composite configuration. The contributing loading parameters, i.e. $E_e V_e$ and $E_f V_f$, are the products of Young's moduli and volumes of the epoxy

$$\frac{\Delta l_a}{l_a}$$

material and the optical fibers. Therefore, the apparent magnetostriction response of the mechanically constrained sensor head, is

$$\frac{\Delta l_a}{l_a} = \left(1 + \frac{E_e V_e + E_f V_f}{E_m V_m}\right)^{-1} \frac{\Delta l_m}{l_m}$$

The above expression implies that for an efficient straining of the magnetostrictive material, the second term in the parenthesis must be extremely small. A practical way to achieve the optimum bonding arrangement for the strain transfer is to apply very small volumes of epoxy and optical materials, while the individual moduli are matched together for the strong cross-linking of the two materials.

2. Improvement of Fiber Optic Interferometer Designs

In order to achieve **Technical Objective 2**, a series of experiments and theoretical evaluations is carried out to increase the senstivity of the fiber interferometer section of the magnetometer system. Interferometric systems based on optical phase sensing use coherent light as the illuminating source. Since detection of very small phase changes is the unique property of interferometers, the noise characteristics of conventional optical sources (e.g. laser diodes and gas lasers) should be controlled for precise measurements. In general, the spatial and temporal coherence of the laser source and the intensity of its radiation must be stabilized for the interferometric response to be optimized. If the laser noise becomes a problem and needs to be eliminated, the feedback method of compensation for quadrature operation (DANDRIDGE and TVETEN, 1981) or the other techniques discussed by DANDRIDGE and MILES (1983) can be used to reduce the noise contribution in the interferometric signal.

Aside from the scattering losses of optical energy propagating in fiber optic waveguides, the main contributing cause of noise in the fiber system is the variation of optical fiber properties (e.g. refractive index, propagational modes and physical

dimensions) produced by randomly fluctuating environmental noise. The temperature-induced noise affecting the phase sensitivity of optical fibers has been investigated by LAGAKOS and BUCARO (1981). Their analysis shows that the proper selection of composition and geometry (e.g. a barium-borate glass in the fiber core) can minimize the fiber thermal variations. In general, the total optical system noise in the interferometer results from laser noise, photodetector noise and environmentally-induced drift. Eliminating signals at the quadrature point can be achieved using a piezoelectric phase shifter (JACKSON et al., 1980). Other detection optimization schemes as discussed by DANDRIDGE et al. (1983) include the alternative active homodyne technique of laser tuning or the two passive homodyne schemes: phase modulation or using a (3 x 3) directional coupler.

The existing interferometric design is improved to achieve a threshold phase shift sensitivity of 10^{-6} radian through noise reduction and electronic signal processing. Broadband noise in the Phase I experimental measurement system limited the minimum detectable signal to 10^{-9} Tesla. As part of the Phase II effort, intrinsic and extrinsic contributions to this total system noise is reduced in a straightforward way. First, the intrinsic noise components of the optical source and detector circuitry is lowered by replacing the helium-neon gas laser source and broadband detector with a stabilized semiconductor laser and a shot-noise-limited PIN diode detector/receiver module. Both of these items are commercially available. Second, extrinsic noise and interference signals caused by mechanical vibration and thermal expansion is minimized by appropriate system packaging. To reduce mechanical vibration interference, the source, detector and sensor head is decoupled from the support package by low-modulus coupling materials. The laser, fiber, fiber couplers and detector is directly coupled, thus eliminating the need for discrete bulk optic components as well as eliminating the interference resulting from the differential motions of such components. To reduce thermal expansion effects, the sensor head packaging is designed so that the signal and reference fiber arms of the interferometer are maintained at as close a temperature as possible. These packaging designs represent an advance in fiber optic magnetometer design. Total noise reduction measured should result in a sensitivity increase of at least two orders of magnitude.

In addition to noise reduction methods, electronic signal processing methods also is applied to optimize the signal detection and estimation process. Two specific techniques is employed. First, conventional dual quadrature interferometric methods is used to dither the phase of the optical field in the reference arm of the interferometer, thereby stabilizing the Q-point of the system. Such stabilization allows the system to operate at the highest possible gain, i.e. under the condition that a small change in applied magnetic field produces the largest possible change in output signal. This stabilization further allows the system to reject slowly varying interference effects. Second, phase-lock synchronization is employed to operate the system at the nulls in the noise spectrum of the system in much the same way as the SQUID system at the Armstrong Aerospace Medical Research Laboratory.

3. Methods to Increase Magnetostrictive Strain Transfer Efficiency

Technical Objective 3 suggests an investigation of the physical methods available to increase the efficiency of the transfer of the strain developed in the magnetostrictive material to the optical fiber. The transfer of strain from the magnetostrictive sensing material to the optical fiber is improved by in-line processing of sensor fiber during fabrication or during subsequent off–line etching and coating. Such processing results in a fiber which is strained optimally along its entire length in response to an applied magnetic field, thus yielding a large output signal response.

In order to engineer such a sensor fiber design, the chemical and mechanical properties of the glass fiber, the METGLAS® sensing material and the coupling agent need to be considered. Strain transfer is increased if a strong chemical bond is created through the glass/coupling agent/METGLAS® interphase. In the manufacturing of telecommunications grade optical fiber or fiber-reinforced polymers, this interphase is typically accomplished by applying monolayers of silanizing agents to the glass fiber prior to coating. This agent optimally couples to the glass surface and, with the proper choice of organofunctional group, to the coating material. In this case, the proper form of the agent which reacts best with both the glass and the METGLAS® surfaces is identified and used. Strain transfer is also affected by the mechanical properties of the fiber, couplings and METGLAS®. The moduli of all coupling materials is made high to keep the strain transfer efficiency high.

Various arrangements of the magnetometer components within the sensor heads are examined using combined coupling of piezo film/magnetostrictive ribbon optical fiber elements. For example, a planar polyvinylidene fluoride/amorphous magnetostriction (PVDF/Metglas®) sensor is built for converting the brain and heart signal magnetic components into the electrical signals. That is, a wire PVDF/fiber sensor is fabricated for the conversion of the electrical signal into precision interferometric signal. The indirect detection of biomagnetic fields is achieved by incorporating these two sensor devices in series within the fiber optic sensor system. The implementation of such a dual-sensing approach can facilitate the application of multiple sensor arrays and multichannel fiber optic magnetometers in "real world" situations.

4. Integrated Optoelectronic Magnetometers

A major improvement in the biomagnetic sensor system is realized in **Technical Objective 4** by integrating source, detector and wave coupling optics onto one opto-electronic substrate. Such a hybrid device reduces system size, reduces interference effects induced by mechanical and thermal expansion and makes a major step towards a convenient, miniaturized all–integrated optical sensor device.

Hybrid Electromagnetic Biosensors

The combination of piezoelectric-based sensing technology with magnetostrictive fiber optic magnetometry can provide a composite probe configuration to enhance the development of the Phase II biomagnetic research. In this application, a mechanically coupled piezoelectric film/magnetostrictive material composite element is placed in series with the sensing arm of the fiber optic magnetometer. The magnetostrictive material can be a selection of Metglas® (Fe-B-Si) alloy or Terfenol-D ($Tb_xDy_{1-x}Fe_y$) compositions. The electronic signals produced by this primary sensor are fed into the secondary piezoelectric tube/fiber optic stretcher in the sensing arm of the interferometer to provide the optical phase modulated detection signals; that is, the biomagnetic signals are actually recorded through multiple conversions of the electromagnetic signal. Such electro-optical conversion techniques can eliminate the need for the extremely large amplification of very weak neuromagnetic signals by electronic amplifiers which inherently contain associated noise levels of some magnitudes. Moreover, the possibility of real-time physiological function monitoring using a cascaded opto-electromagnetic transformation approach becomes more apparent. Indeed, the preliminary testing of such combined piezoelectric and magnetostrictive sensor heads has already been performed in a recent laboratory experiment. Several series of tests are conducted to demonstrate the performance of piezoelectric film/Metglas® composite sensors as the primary magnetic sensing elements. The output signal of such a transducer is used as a modulator to drive the piezoelectric/optical fiber stretching coil in the experimental interferometric magnetometer. So far, encouraging results have been observed.

5. Application of Sensor Array and Gradiometer

Technical Objective 5 is achieved through a detailed study of magnetic field distributions in a variety of fiber optic sensor heads. The composite materials in the magnetic sensing elements of the magnetometer consist of magnetostrictive metallic glass and the single–mode optical fibers. The mechanical bonding of the composite sensor head is made of no-field annealed METGLAS® samples with high elastic modulus using a low elastic modulus epoxy adhesive. The coupling adhesive applied at limited contact places effectively transfers the magnetically-induced mechanical strain to the high modulus silica fiber. The hybrid combination of optical fibers and magnetostrictive strips in different configurations is constructed and tested for sensitivity to radial and tangential spatial distributions of the biomagnetic fields.

The inherent shielding nature of the two transducer elements, i.e. the high electrical resistivity of METGLAS® alloys and the electromagnetic immunity of the optical fibers, makes the application of such sensing materials suitable for hostile environments. For example, in space the materials shields against plasma-discharged electrostatic potentials; in battlefield conditions the material tolerates electromagnetic pulses. Complete shielding against all degrading physical factors,

e.g. high temperatures and radiation effects, is considered using special coating materials in order to make the sensor more rugged. Moreover, shielding methods against very high magnetic fields is taken into account so that the magnetization would not occur and so that the structural integrity of the stiff metallic glass element would not be damaged through annealing and hardening effects.

For environmental shielding purposes, the temperature and vibrational stability of electromagnetic sensor heads can be accomplished by a transducer coating of low thermal conductivity/diffusivity materials and ruggedized packaging with low elastic modulus RTV silicone rubbers. Although the laser interferometric sensors have an inherently broad frequency response, the frequency response of candidate magnetostrictive materials is rather limited. Both piezoelectric and magnetostrictive materials undergo mechanical resonances and their response sensitivity decreases as the frequency of the excitation signal increases. However, both sensor materials have relatively short time constants (<ms) and reliably respond to the neuroelectric/magnetic frequency range of below 50 Hz.

For steady operation in the presence of background magnetic fields, specially-designed double magnetic sensing heads is incorporated into the magnetometer. In this system the reference arm of the optical fiber in the interferometer is bonded to a separate magnetostrictive element so that the magnetometer consists of two identical probing heads. If one sensor head is subjected to the field to be measured while the other companion pair is placed near the sensing head, the effects of unwanted magnetic fields is automatically cancelled. This is caused by the inherent action of an interferometer that senses magnetically induced phase-shifts; one sensor head contains both the signal and the noise magnetic fields while the other contains the noise field only. Such a "tandem" configuration allows the magnetometer to operate as a gradiometer in which the variable spacing between the two sensor heads control the measured gradient parameters. The successful performance of the double sensor head design is the basic foundation for the development of the high-spatial-resolution sensor arrays made of a series of magnetic probes.

6. Acquisition of Families of Test Data

To achieve **Technical Objective 6**, families of test data is acquired. For the simulated testing measurements, a programmable random-waveform function generator is used to excite the magnetizing coils in the magnetometer. In laboratory field conditions, human biomagnetic fields is used to examine the response characteristics of the device. A series of calibration experiments is performed to simulate the detection of magnetic fields with extremely low amplitudes and complex waveforms. Methods of reducing the noise source and compensating for temperature variation is implemented in the prototype system. An arbitrary waveform generator (Data Precision 2020) is used to produce complex repetitive signals for analysis by the laser stimulated fiber optic interferometer. This device is capable of producing a 5 mV peak–to–peak signal corresponding to an algebraic polynomial function. This device is used extensively to generate current dipole

sources for magnetic field detection. Similar tests are performed for a variety of specially configured magnetometer arrangements; for example, a gradiometer configuration is tested using a pair of magnetic sensing elements in the fiber optic arms of the interferometer, and spatial distributions in biomagnetic fields is evaluated using arrays of sensor heads.

Magnetometer Sensitivity and Signal-to-Noise Ratio

The following paragraphs discuss the practical instrument limitations along with the means of employing a hybrid magnetostrictive fiber optic-based sensor for the prototype demonstration of human neuroelectromagnetic and very weak magnetic signal measurements as low as 10^{-14} Tesla. In particular, the minimum detectable sensitivity of the fiber optic interferometric magnetometer has been defined. Based on the previous theoretical calculations made at American Research Corporation of Virginia, the minimum detectable magnetic field signals were found to be on the order of 10^{-16} Tesla per meter of magnetostrictive sensing optical fibers. The intrinsic noise sources of the basic sensing elements, e.g. magnetostrictive materials including the single-mode optical fibers, are generated due to perturbations in temperature which change the physical dimensions of these sensor materials. However, the change in refractive-index of the silica core-cladding fibers due to temperature fluctuations which may affect the optical waveguide propagation characteristics are actually insignificant compared to other physically-induced disturbances. The effects of eddy current loss and hysteresis in the selected magnetostrictive materials are also insignificant compared to environmentally degradating noise sources. The major sources of noise signals in the proposed magnetometer device besides the optical and photodetector shot-noise-limited fluctuation levels are the environmentally-induced thermal, vibrational and background magnetic disturbances.

It is desired to reduce and ultimately eliminate these omnipresent noise signals accompanying the actual biomagnetic signals. The recovery of very small magnetic signals from environmentally-induced large signals has been performed through the combination of passive common-mode-rejection (gradiometry) techniques and appropriate sensor package insulation with special ruggedizing coating materials to be implemented later. Although the presence of residual noise signals in the experimental fiber optic interferometric magnetometers has significantly limited the ultimate detection sensitivity, a practical signal-to-noise ratio corresponding to magnetic sensitivity of a few femtoTesla/$\sqrt{\text{Hz}}$ has already been observed in the laboratory using the Mumetal-based magnetically shielded chambers. This signal-to-noise ratio is being improved by an electronic phase-lock synchronization technique in which the magnetometer is operated at the null in the noise spectrum of the sensor system response. That is, the signal-to-noise ratio is maximized for selected narrow bandwidths in the magnetometer background noise.

As in the case of magnetostrictive fiber optic transducer stabilization, the electromagnetic-based probes either in the form of a piezoelectric/fiber sensor configuration or in the form of a piezoelectric/magnetostrictive sensor configuration for the magnetometer device is compensated against environmental noise sources through passive tandem transducer arrangements (gradiometer) and/or shielding with high permeability materials.

Biomagnetic Fields and Omnipresent Magnetic Noise Levels

Conventional biomagnetic instrumentation has made possible the study of magnetic fields emanating from many organs of the human body. Such methods can describe and evaluate brain disorders and other physiological functions. In addition, new techniques are sought to improve magnetometer instrumentation for studies of brain functions related to responses to sensory stimuli, motor activity and thought processes. However, background magnetic noises which reduce the sensor signal-to-noise ratio limit optimal operation of biomagnetic instrumentation. **Figure 3** represents the typical levels of human body magnetic fields and the associated background magnetic fields as well as the range of detectability by ultra-sensitive fluxgate or cryogenic SQUID magnetometers. The most serious problem for any such instrument including fiber optic-based magnetometers is transient ambient magnetic noise such as the earth's magnetic field. Therefore, methods must be found to reduce the ambient magnetic noise to below a few femtoTesla over the period of biomagnetic testing experiments. Background ionospheric and magnetospheric magnetic field noise gradients of about 1 picoTesla/cm must also be eliminated.

For these reasons, both passive and active magnetic shielding techniques are considered. For example, higher-order gradiometry and/or environmentally shielding techniques based on appropriate magnetic materials (e.g. Mumetal 77Ni, 5Cu, 2Cr) are utilized. However, at very low frequencies the noise amplitude increases at a slightly faster rate than the inverse of frequency relationship (i.e., 1/f). Hence, the effect of ambient magnetic noise which may seriously restrict the ability to measure very slowly changing biomagnetic signals is ultimately reduced by the first- and second-order gradiometric configurations. Excess noise from the power line fundamental frequency and its harmonics can eventually be removed by comb filters. Alternatively, the use of a digital matched filtering technique is employed so that the peak signal-to-noise ratio is maximized. It is expected that the matched filter design on appropriately-weighted data can provide signal-to-noise ratio improvements of several tens of decibels (dB). Computer software techniques for reduction of noise (digital filtering) is implemented.

Computer Techniques for Biomagnetic Signal Analysis

Comprehensive analysis of signal response characteristics are performed for the magnetometers. Specific biomagnetic data analysis and display procedures include amplitude analysis, spectral (e.g. fast Fourier) transformation, magnetic field contour mapping and cross-correlation techniques. The amplitude analysis was performed by showing the magnetometer output signal (waveform) in time domain. Since the A/D conversion resolution of the signal analyzer is 14 bits, biomagnetic waveforms can be displayed with 61 μV vertical resolution within ± 500 mV full scale. The time dependent amplitudes of the digitized waveform, can directly be related to the amplitudes of biomagnetic signals in terms of sub-microTeslas. The spectral information related to the waveforms is shown by obtaining power spectrum of the detected signals. Actually, the frequency-domain analysis is performed in terms of the power spectrum. Herein, output magnitude indicates the average power per Hertz. A Hanning window is used in the digital calculations.

In addition to amplitude analysis and power spectrum representation, other signal processing techniques such as auto-and cross-correlation functions are used for the purpose of signal comparison with the biomagnetic measurements. Both the lateral distribution (two-dimensional contour mapping) of the magnetic fields and the vertical location of the current source within skull and/or chest cavity can be determined using the correlation methods. All of the mathematical calculations related to data analysis and reduction including signal averaging, average frequency, amplitude and RMS values are provided from the front panel buttons.

7. Optimization of Proof-of-Concept System

Technical Objective 7 requires the optimization of a proof-of-concept fiber optic magnetometer system based on the findings of the Phase II program. Particular emphasis is given to the design of an integrated, compact, fiber optic magnetometer and a programmable multiplexed array for biomagnetic field evaluation in the commercialization phase of the program or in government sponsored development for the operating divisions. Questions to be addressed include sensor head configurations, trade-offs between maximum sensitivity and the requirements for extensive signal processing, reduction of interfering signals, system reliability, cost, size and weight, susceptibility to impact damage, acceleration or electromagnetic pulse. Consideration is also given to the suitability of the optimized system for eventual integration of the components.

The approach to the proof-of-concept system includes developing of a high resolution interferometer with electronic processing to reduce system noise, using annealed coated fibers, shielding system components from environmental noise, using rigid and planar circuitry to reduce vibration effects and employing second-order and third-order gradiometer systems. As noted earlier, the sensitivity of a fiber optic interferometer can approach 10^{-6} radian using low-noise photodetectors and lasers stabilized with respect to frequency and amplitude. The Phase II program improves the insertion loss and power split of fiber optic couplers. Additional considerations include the integration of fiber and output connectors to minimize output losses through the purchase of fiber detectors with pigtailed connections.

The test data obtained in achieving Technical Objective 6 is used to generate the technical specification for an engineering model to be developed in Phase II of the program. The final design and optimization makes use of experimental results obtained from magnetocardiography and evoked potentials in human subjects. Favorable results in these areas would encourage a commercialization effort in Phase III of the program.

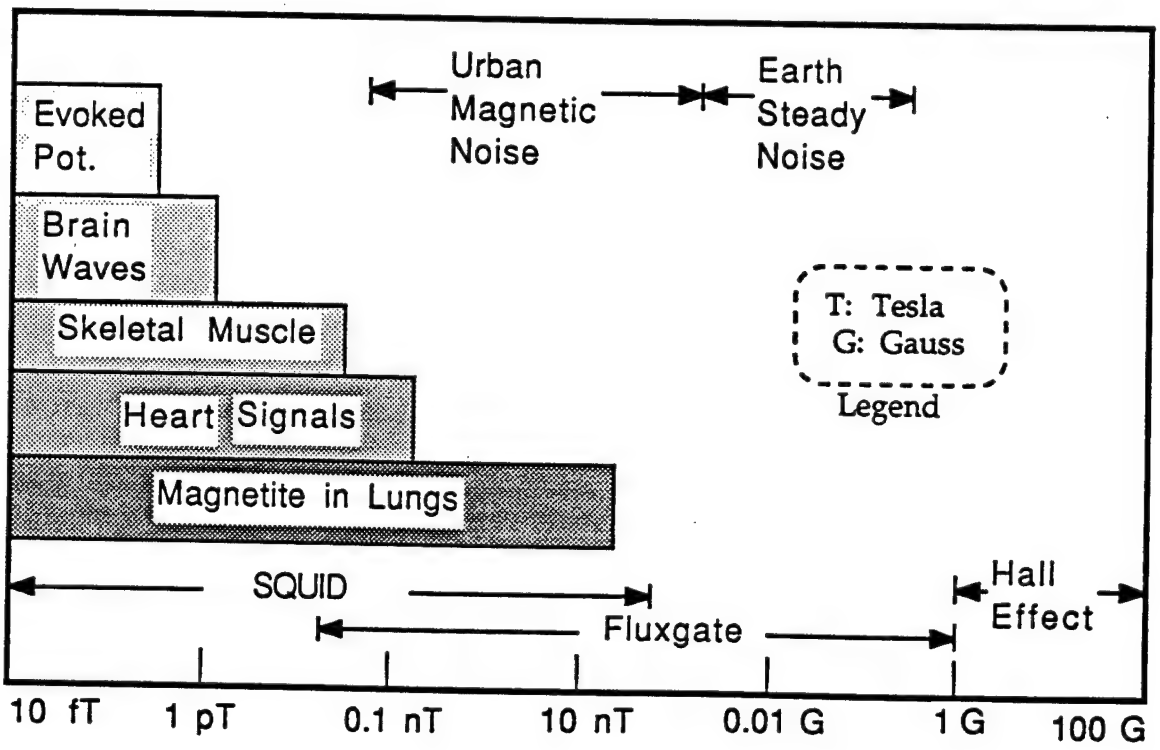

Figure 3. Magnetic Levels of Body and Background Magnetic Fields and Detection Range of Conventional Magnetometers.

VI. RESULTS AND DISCUSSION

The following sections include the experimental work, test procedures, results and discussion of work accomplished during the Phase II program.

1. Fiber Optic Interferometric Magnetic Field Sensor and Biomagnetic Computer Modeling

Work performed under the first technical objective of the program involved extensions of theory and computer modeling to describe the response of hybrid magnetostrictive/fiber optic interferometric sensors to human biomagnetic fields. Theoretical extensions pertaining to magnetostrictive materials interacting with fiber optics were performed under subcontract at the Fiber and Electro-Optics Research Center at Virginia Polytechnic Institute and State University (VPI&SU) and were submitted as a report by DUNCAN, et al. (1988). The first subsection under this heading gives a brief discussion presented in this report from the subcontractor to the American Research Corporation of Virginia (ARCOVA). Theoretical treatments leading to suggestions for design improvements for the fiber optic Mach-Zehnder interferometer were also performed under subcontract at VPI&SU and are presented in a report by SUDEORA (1988) to ARCOVA. Major conclusions drawn in this report are presented in the second subsection. Computer modeling of human biomagnetic fields was performed at ARCOVA. Results derived from these models are presented in the third subsection under this heading.

Fiber Optic/Metglas ®Magnetic Field Sensors

Through consideration of fiber optic Mach-Zehnder interferometry and the response of magnetostrictive amorphous metal alloys to magnetic fields, several findings have been realized regarding the limitations and possible geometries of fiber optic/Metglas® magnetometers. In particular, noise from thermal effects and electromagnetic eddy currents within the metallic glasses places a lower limit on the magnetic field strength at which magnetostriction takes place. This limit has been calculated to be 3×10^{-15} Tesla (T). With this magnetostriction limitation and several assumptions concerning the construction of the interferometer, including an interferometric phase sensitivity of 10^{-6} radians, theoretical calculations lead to a minimum detectable AC magnetic field of 4×10^{-13} T per meter of sensing optical fiber. This is sufficiently sensitivity to be able to detect both human magnetocardiographic (MCG) and magnetoencephalographic (MEG) fields.

Fiber Optic Mach-Zehnder Interferometry

Several suggestions for improvements to the fiber optic Mach-Zehnder interferometer in use at ARCOVA have been presented by the subcontractor at VPI&SU. In particular, the two optical fibers forming the sensing and reference arms of the interferometer should follow similar paths to reduce noise from

mechanical sources. Temperature related disturbances are a primary noise source, so the optical fiber should be mounted on heat sinks and coated with heat insulation to minimize temperature variations. In addition, in order to observe a stable and repeatable output signal for an optimal detection sensitivity and a large dynamic range, it is necessary to incorporate two feedback control loops in the Mach-Zehnder interferometer. One feedback loop is used to achieve a stable quadrature point operation while the other feedback loop provides a signal-nulling DC magnetic bias field to detect small changes in the DC or low-frequency fields to be measured.

Human Magnetoencephalographic/cardiac Fields

The two areas of human biomagnetic fields under study in this program are the heart and brain-induced fields. The heart fields are probably the most promising for sensor development because they are at least an order of magnitude stronger than the brain fields, and are consistent, predictable and repeatable. Recorded MCGs and MCG maps of simulated (modeled) heart fields can be found in WILLIAMSON, (1983). These models are rather complicated because of the complex geometries of the body and the physiological measurements needed to map these geometries.

As presented in the first interim technical report, the simulated human magnetoencephalographic/cardiac fields were displayed by a contour mapping program. The model used to map the heart-induced field is that of CUFFIN and COHEN (1977). The model represents the chest wall as a semi-infinite volume conductor and the heart signal as a dipole current. For modeling of brain-induced field, the skull is considered to be a spherical conductor volume. The formulas used for computing the brain fields were taken from WEINBURT (1984).

The magnetic field is calculated from the Biot-Savart law and the field is caused not only by the dipole, but the electric field current carried by the conducting volume. The equations for magnetic field components were programmed in a microcomputer. The program for computing the fields was developed from numerical modeling. The output of this program is 256 x 256, two-byte-integer map of the magnetic fields which can be observed with a plotting program. Figures 4-7 show the photographic representation of computer-generated contour maps for radial and tangential components produced by heart and brain fields. For the simulation of the heart fields, a dipole source of 0.05 Ampere-meter was located behind (0.05 meter below) a semi-infinite conductive slab (0.1 meter x 0.1 meter) and oriented from left to right. For the simulation of the brain fields, the dipole source of 2×10^{-6} Ampere-meter was located 0.05 meter below the skull of 0.1 meter radius. The dipole orientation for the brain field representation was in the upward direction with respect to the computer display. The photographs presented in these figures were taken from color contour maps on the screen of an IBM PC AT-compatible computer with an enhanced graphics adapter and color monitor.

2. Improvement of the Fiber Optic Interferometers

The fiber optic biomagnetic sensor is based on Mach-Zehnder configuration responses to the optical phase difference between the two fibers (sensing and reference arms) of the interferometer. The interferometric magnetometer, in addition to being sensitive to the low-level biomagnetic signals, responds to high-level noise signals due to fluctuating environmental disturbances; that is, interferometers usually respond to unwanted environmental perturbations such as temperature, air flow and acoustic noises. Such inherent noise sensitivity produces a differential optical phase shift between the two fibers of the interferometer which in turn reduces detection sensitivity to the magnetic field of interest. There are several different demodulation schemes which can be used to recover the signal from the drifting environmental noise. The following paragraphs describe the problem of signal fading and review the approach for quadrature-point stabilization schemes when homodyne demodulation technique is used. A piezoelectric tube/fiber stretcher (phase shifting) method is used to maintain the interferometer at maximum detection sensitivity state.

As was mentioned above, the response of the interferometric sensor is related to the phase difference between the two optical fibers of the Mach-Zehnder interferometer. The interference phenomenon resulting from the recombining fiber coupler converts the phase modulation into optical intensity modulation. The optoelectronic photodetectors incorporated in the interferometric system, in turn, respond to intensity variations.

In general, the photodetector current, i (t), corresponding to time-dependent intensity fluctuation is given as

$$i(t) = C\left[1 + \cos \phi(t)\right]$$

where C is a function of optical power, detector quantum efficiency and interferometric fringe visibility; $\phi(t)$ is time-dependent phase shift; and cos is a trigonometric cosine function. The response of the detected light intensity to changes in relative phase between the two fibers of the interferometer is obtained by differentiating the above equation, i.e.,

$$di(t) = \sin \phi(t)\, d\phi(t)$$

In the interferometric magnetometer, the sensing fiber is coupled to the magnetostrictive material, so that the optical phase difference of interest is modulated by the low-level biomagnetic fields. The phase shift values can conveniently be extracted when the photodetector response is linear, i.e.,

$$\sin \phi(t) = 1$$

The condition stated in the above relationship implies that the relative phases of the two fibers be in quadrature (e.g. $\pi/2$), so called, the "quadrature condition." When the interferometric signal response is biased at the quadrature point, the relationship between the incremental phase change and the incremental intensity change is linear and maximum. However, maintaining the interferometer at quadrature is far from trivial. For example, temperature fluctuations produce a phase shift on the order of 100 radians/°C per meter of fiber. Such problems are typically due to the thermal expansion of the silica fibers. The drift causes changes in the amplitude of the output signal (i.e. signal fading). Under certain conditions the output signal may even be zero (e.g. $\sin \phi (t) = 0$).

For the homodyne demodulation scheme used in the interferometric magnetometer system, quadrature-point stabilization is obtained by active servo feedback electronic circuits. Such a compensator device allows the interferometer to be maintained at a constant working point by control of the voltage to the piezoelectric modulating element.

The compensator system consists of two parts: the feedback circuit and the piezoelectric tube (PZT) element. The PZT which has a number of turns of fiber around it, controls the length of the reference arm of the interferometer. Modulation of the PZT element controls the optical pathlength difference and thus the phase difference between the arms; a change in the PZT element diameter translates into a change in the pathlength of the reference arm. The diameter of the PZT is varied by the feedback circuit such that the optical phase difference between the two arms of the interferometer is always $\pi/2$ radians or its odd multiple. Figure 8 illustrates a schematic diagram of the compensator. The feedback circuit consists of a differential amplifier, low pass filter, integrator and an inverting amplifier. The inputs to the differential amplifier are fed from the two detector outputs of the interferometer which are out of phase by π radians. These outputs when converted to voltages are

$$V_1 = V_A + V_B \cos \phi$$

and

$$V_2 = V_A - V_B \cos \phi$$

where the voltages, V_A and V_B, are proportional to the laser power. The differential amplifier amplifies the difference between its two inputs to yield

$$V_{01} = V_1 - V_2.$$

Substituting V_1 and V_2 into the above equation results in the output of the differential amplifier as

$$V_{01} = 2V_0 \cos \phi,$$

where V_B has been replaced by V_0.

Typically, input signals having frequencies up to about 90 Hz are passed with no attenuation while signals above 90 Hz are attenuated (NADER et al., 1990). There is also little phase difference between the input and output signals of the low pass filter up to about 40 Hz; therefore, V_{02}, the output of the low pass filter, is an exact reproduction of the V_{01}, the input of the low pass filter, up to about 40 Hz, i.e.,

$$V_{02} = V_{01} = 2V_0 \cos \phi$$

In addition, all input signals above 7 Hz have a phase lag of π radians at the integrator output compared to the input. Signals below 3 Hz do not have any appreciable phase change while signals between 3 and 7 Hz have phase shifts between 0 and π radians. Thus, for all practical purposes the circuit acts as an integrator for all input signals above 5 Hz and the output of the integrator, V_{03}, can be represented by

$$V_{03} = 2V_0 \sin \phi$$

This output of the integrator is valid for all signals between 5 and 40 Hz. However, temperature and low frequency vibration noises may exist in this frequency range. The output of the integrator is amplified and applied to the PZT. The component values of the inverting amplifier are selected such that the output does not saturate, while at the same time being as close as possible to the saturation voltage.

As the optical phase between the arms drifts because of environmental noise, the detector output follows this variation as a cosine function. The output of the feedback circuit also follows this variation, but with a phase lag of $\pi/2$ radians, i.e., as the sine of the optical phase variation. This output when applied to the PZT controls the length of the reference arm such that the optical phase difference between the arms of the interferometer is always $\pi/2$ radians or its odd multiple; the interferometer is stabilized at quadrature.

3. Methods of Fabrication of the Sensor Heads

The experimental testing of magnetic sensing elements was performed by fabricating and subsequently evaluating a series of composite sensors made of the hybrid combinations of single-mode optical fibers, polymer piezoelectric (PVDF) transducers and magnetostrictive materials. Some of the special configurations of laboratory-constructed field sensing elements were as follows: single-path or multiple-path fibers bonded with epoxy adhesives to planar or cylindrical samples of amorphous metallic glass (Metglas®) sheets; short fibers coated with powdered Metglas® alloy PS-21 (Fe_{78} B_{13} Si_9) or the new rare-earth metals magnetostrictive materials (Tb, Dy, Fe) using the vacuum evaporation technique; and PVDF sheets coated using the above technique. The preliminary results of the measured output responses of these sensors indicated that all of the above composite elements were indeed magnetic field detectors with different degrees of sensitivity. In particular, the mechanically coupled fibers with their unjacketed spots bonded at entering and exiting edges of Metglas® ribbon were found to be about an order of magnitude more sensitive to the applied fields as compared to the spot bonding of the fibers through the polymer jacketing material. The information obtained as a result of these findings helped the optimal fabrication of a new generation of compact magnetic field sensors implemented in magnetometer research instrumentation. Figure 9 represents a geometric configuration of a typical multi-layer cylindrical-based sensor head.

Annealing of Metglas® samples was also considered for improved response in magnetic sensing components. The objective is to obtain macroscopic uniformity of local magnetic orientations. This can be achieved by reducing local and structural stress levels to where the applied field can induce uniaxial magnetic anisotropy. The procedure for the annealing process usually includes physically subjecting the Metglas® samples to high temperatures near the Curie temperature and to large magnetic fields of a few thousand Ampere-m^{-1} for a period of about two hours. The annealing setup designed to provide the optimal Metglas®-based elements used in fiber optic magnetometer sensor heads consisted of an Argon pressurized tank for an inert-gas environment, a tubular furnace, a set of concentric Pyrex glass tubes and a high-amperage DC power supply. The inner tube is surrounded with a coil to provide the needed annealing magnetization strengths. Specific annealing parameters tested on several Metglas® ribbons during this period were:

Samples	~	planar 2605-S2 materials
Environment	~	Argon gas at atmospheric pressure
Applied Magnetic Field	~	14,000 Ampere-m^{-1}
Annealing Temperature	~	400° C
Annealing Time	~	7200 Seconds
Coil	~	210 turns and 0.22 meter long

The majority of samples were annealed along their transverse direction (relative to the length of the ribbon) with the magnetic field perpendicular to the ribbon axis so that the magnetic easy axis could be defined along the width direction. The response of these transversely and longitudinally annealed sensors, to be reported later, is expected to increase magnetic detection sensitivity by at least an order of magnitude.

The pigtailed "tandem" sensor heads having fibers of approximately 3 meters in length (similar to 2 meters for the He-Ne laser magnetometer sensors) were attached to the optoelectronic module through four fiber lines. Splicing was achieved using a single-mode fiber portable fusion splicer (Model FW 304, Orionics, AMETEK). Application of the fusion splicer was found to be an important factor in compact packaging and reliable system operation since efficient coupling values could not be obtained using conventional mechanical splicers. Splicing loss for the slightly different size (dissimilar) fibers (70 and 85 μm cladding diameters) used in this magnetometer was found to be about 3 dB. In the case of He-Ne laser magnetometer fiber splicing, the best splice for the 125 μm fiber (10 μm core, 125 μm cladding) was obtained when a 2-second discharge arc at 60 mA was applied across the bare fiber ends with 6 μm face-to-face gap. The fusion splice losses for these similar (125 μm into 125 μm) fibers were found to be negligible compared to typical 25 dB loss due to the laser beam-to-fiber coupling.

4. Present Magnetometer Technology at ARCOVA

The present fiber optic interferometric biomagnetic field sensing instrument incorporates several features improved over the previous systems. Such desired design considerations already implemented are: two compact and a subcompact magnetometer packages; integration of hybrid electromagnetic sensing elements; and application of active quadrature-point interferometer stabilization. The following subsections describe the technical specifications and the state of ARCOVA technology.

Instrumented Manikin

A prosthetic manikin including torso and head sections was acquired for biomagnetic simulation testing using the laboratory-prototype bioengineering fiber optic interferometric magnetometer. This manikin is made of non-magnetic urethane foam which does not perturb the fields. Instrumentation of the manikin began with incorporation of compact current sources within the chest cavity and the skull for cardiac and neuromagnetic signal simulation, respectively. The electric current source simulating the brain waves is a compact solenoid coil attached to the inner wall of the manikin head. The attachment was provided by Velcro® strips which facilitates positioning adjustment of the coil. This magnetic field generating solenoid has geometric characteristics of 1.125 inches in length and 0.25 inches in diameter with 65 turns of wire. The driving current is provided by the signal generator (Data Precision®, Model 2020) which can supply up to 0.1 A (rms) electric

current into the coil. The coil having low resistance is connected in series with a 31Ω resistor. Therefore, the maximum magnetic field intensity produced at the center of the solenoid is about 0.3 nT (rms). This corresponds to twice the amplitude at the two solenoid tips, e.g., magnetic induction at the ends is about 0.15 nT (rms).

Since the magnetic field amplitude decreases as a function of distance squared from the coil axis, the intensity of magnetic fields in the vicinity of the coil is expected to be several orders of magnitude lower than the central magnetic field level. For example, when a root mean square current of 70 mA at 10 Hz is applied, the magnetic field intensity at 1.27 cm from the coil axis is found to be about 8 μT (rms). The manikin was also instrumented for simulating the cardiomagnetic signals, e.g. similar to the brain wave excitation coil, a compact solenoid coil was placed inside the chest cavity of the manikin. A power amplifier box for driving the magnetic field generating coil was constructed. The basic components of this current amplifier circuit are a MOSFET operational-amplifier (Model IRF 511) and a potentiometer. The box is externally connected to the excitation coil of 1 inch in length, 0.25 inch in diameter, 56 turns, negligible resistance and 100 μH inductance. In performance testing, a sine wave (5 Hz, 350 mV (rms)) input to the box can drive a current of 131 mA (rms) into the coil. This current corresponds to a magnetic field amplitude of about 360 μT (rms) at the center of solenoid. On the opposite side of the chest wall (2.5-inches thick) where a portion of the magnetic field is "seen" by the sensor head, the field amplitude is estimated to be ~ 3 μT.

The instrumented manikin with existing coils was utilized for measuring biomagnetic field signals. For the purpose of correlation and mapping measurements, two plastic grids (5 x 5 mesh) were attached on the interrogation areas of the head and chest.

He-Ne Based Compact Magnetometer

A portable magnetometer based on a He-Ne laser system was constructed. This fiber-optic-interferometric based magnetometer was assembled onto an optical rail of 4-inches by 12-inches dimensions. The system incorporated a small optoelectronic device aside from the He-Ne laser and the two sensor heads. This fiber-optic-interferometric module consists of three main optoelectronic elements: 1) two fiber couplers (2 x 2 parts, 630 nm cut-off wavelength for single-mode operation), 2) a piezoelectric ceramic tube with multiple fiber turns to be used for the interferometric output optimization (quadrature-point operation and/or calibration), and 3) a dual-element photodiode PIN detector for receiving the two complementary interferometric output signals.

The He-Ne laser beam output was injected into a micro lens and 5-axes fiber positioner for laser beam-to-fiber power coupling. The entire magnetometer device consists of three main subsystem modules, namely: a laser power supply; tandem sensor heads; and a hybrid optoelectronic/fiber package. **Table I** lists the subcomponents used for the system fabrication. **Figure 10** illustrates the detailed configuration of the optoelectronic module components.

Laser-Diode Based Compact Magnetometer

A hand-held magnetometer based on semiconductor laser-diode system was completed. This magnetometer system consists of three main subsystem modules: 1) laser-diode power supply, 2) tandem sensor heads and 3) hybrid optoelectronic/interferometric fiber optic package. The entire magnetometer has a volume of 2" x 2" x 7". The optoelectronic module consists of a semiconductor laser diode, two fiber couplers (2 x 2 ports), two photodiode PIN detectors and coupling optics for efficient launching of laser diode beam output into the single-mode fiber. **Table II** lists the components used in packaging the complete device. **Figure 11** illustrates a perspective view of the laser-diode based system.

Subcompact Magnetometer

A subcompact magnetometer package was constructed. This hand-held MCG/MEG device consisted of a laser-diode, a microlens, two optical fiber couplers, a dual-element photodiode detector and a clear plastic housing. The mechanical assembly of the laser-diode-to-fiber coupler and fibers-to-photodiode launching were fabricated in a specially engineered packaging configuration. Except for the associated sensor heads, all components were packaged inside a small tube (1.25-inches diameter, 12-inches length). **Figure 12** shows a photograph of the subcompact magnetometer device.

Two magnetic field sensor heads were fusion spliced to the laser diode-based subcompact magnetometer. Each of the selected sensors was made of three-serially connected sandwiches (Metglas/fiber combinations). The sensor head packages were fabricated in the subcontractor's facilities. The sensors had pigtailed fibers of 10 (μm)/125 (μm) which were dissimilar with the 4 (μm)/80 (μm) fibers used in the interferometer. However, good coupling efficiencies of about 35% could be obtained by various combinations of fusion spliced fiber core/cladding diameters.

5. Special Sensor Head Configurations and Serial Array

Evaluation of various sensor head geometries and their subsequent response characteristics was performed by the Fiber and Electro-Optics Research Center (FEORC) at Virginia Polytechnic Institute and State University (VPI & SU). The focus of the recent effort was to investigate the repeatability of the sensor fabrication processes so as to obtain sensors of near identical sensitivities and also to obtain the response of a multiple-array sensor head consisting of three individual sensors in series. Implementation of such a multiple-point sensor array detector head improved the sensitivity measurements.

In order to compare with the previous findings at ARCOVA and/or FEORC, the sandwiched sensor head configuration was chosen; that is, the characteristic performance tests used sensors in the form of a planar structure sandwiched with a few turns of fiber enclosed between two layers of Metglas® sheets. As was mentioned above, the first aim was to test the repeatability of the sensor fabrication

process. Ten (10) identical sensors were constructed and tested for their detection sensitivities. Each sensor incorporated 60 cm of fiber in the form of nine (9) passes sandwiched between two layers of Metglas® sheets (7 cm X 1.25 cm). The second aim was to build a multiple-array sensor consisting of three of the best sensor heads (connected in series) in the sensing arm of the fiber optic interferometric magnetometer. A Mach-Zehnder interferometer was configured as a gradiometer with three more sensors in series in the reference arm.

A comparison of the sensitivities of the ten (10) sensor heads shows that good repeatability is obtainable even with the manual fabrication process. Seven of the ten sensors provided detection sensitivities on the order of 10^{-3} radian/Tesla. Here, radian is the resultant phase shift of the interferometer for a given magnetic field intensity. The lower sensitivities of the remaining three sensors could be attributed to factors such as excessive amounts of epoxy used and improper tension applied to the fibers. The detection sensitivity of this multiple sensor head configuration (e.g. 5×10^{-3} radian/Tesla) was the highest obtained thus far at FEORC. The results of this multiple sensor head testing show that the multiple-point sensing is a viable configuration for detecting very low level biomagnetic fields.

6. Laboratory Simulated Biomagnetic Field Measurements

Evaluation of various simulated biomagnetic signals including interferometric detection, data reduction and graphic presentation was performed. The experimental procedures undertaken were similar to the approach described in the previous interim technical report. However, expansion of computer techniques including additional measurements were accomplished for improved presentation of simulated and/or measured biomagnetic fields within the instrumented manikin. The following subsections provide the typical observation of simulated biomagnetic signals, using the instrumented manikin, fiber optic interferometric compact magnetometers and computer-aided graphic programs.

Data Acquisition

To perform an experimental prototype demonstration, families of test data have been acquired. For simulated testing measurements, a programmable random-waveform signal generator has been used to excite the magnetizing coils in the magnetometer. In laboratory field conditions, simulated human biomagnetic fields have been used to examine the response characteristics of the device. A series of calibration experiments has been performed to simulate the detection of magnetic fields having extremely low amplitudes and complex waveforms. Methods of reducing the noise source and compensating for temperature variation have been implemented in the prototype system. An arbitrary waveform generator (Data Precision® Model 2020) is used to produce complex repetitive signals for analysis by the laser fiber optic interferometer. The function generator is capable of producing a 5 mV peak-to-peak signal corresponding to an algebraic polynomial function. This device has been used extensively to generate current sources for biomagnetic field

excitation. Parametric studies of the experimental results have been obtained for analysis and comparison with the conventional neuro- and cardio-biological measurements available in the literature. Similar tests have been performed for a variety of specially configured magnetometer arrangements; for example, a gradiometer configuration has been tested using a pair of magnetic sensing elements in the fiber optic arms of the interferometer. In addition to real-time analog signal analysis, computer techniques such as the Fourier transform have been applied to the detected signals.

Figure 13 shows data acquisition components used in this project. These components, labeled alphabetically, are: a) differential amplifiers, b) lock-in-amplifier, c) signal analyzer, d) simulation function generator, e) microprocessor with a monitor and f) hard copy signal plotter.

Results and Data Presentation

For the experimental measurements dealing with the instrumented manikin (with the biomagnetic simulating excitation coils), the noncontacting sensor heads were positioned at a distance of about 2-3 inches form the magnetic excitation coils. **Figures 14 and 15** show the driving signal and the several repeated responses for the simulated heart signals using the laser diode-based compact magnetometer. Herein, only the differential amplifier was used for the output signal amplification and filtering. In Figure 8, the power spectral function (d) of the output closely resembles the corresponding function (b) of the cardio (P-QRS-T wave) input signal. This established the reliability of the interferometric magnetometer instrument. Alternatively, **Figures 16 and 17** show the driving brain signals and the corresponding output signals for the simulated alpha rhythm (continuous wave at 10 Hz) and beta rhythm (continuous wave at 20 Hz). **Figure 18** show the output responses for the same two input simulated brain signals using the lock-in amplifier at the back end of the magnetometer. Therein, smoothed and enhanced output waveforms were observed.

To find out the system signal-to-noise ratio (S/N) for the measured biomagnetic simulation signals, the floor noise at the frequencies of interest (where the power spectrum functions peak) were recorded and later compared with the signal peak values. **Figure 19** shows the output responses in which the differential amplifier or the lock-in amplifier were in line. Typical S/Ns were found to be in the range of 5,000-10,000 for both heart and brain detection. However, the best S/N of 500,000 was observed from a heart measurement. Such high S/N resulted in minimum detectable biomagnetic field intensity of about 10 picoTesla.

Two-dimensional scanning measurements were also demonstrated on the instrumented manikin. However, because the scanning was performed manually, only a 3 x 3 grid was actually used. In order to increase the S/N and present the amplitudes or spectral data in averaged values, a digital filtering technique was incorporated. The specially written program uses integer-based spatial oscillations

to pass and to suppress all high frequency oscillations. Since the operator has a 3 x 3 data-point extent, high frequency oscillations include large magnitude changes within a 3 x 3 matrix. Such operation tends to smooth the measured biomagnetic field contour maps and increase the uniformity of the raw data. The operator is used by computing a weighted average on each spatial point and the closest of neighboring points. Thus, the center of the operator matrix is aligned with the spatial point to be processed. However, when a very course scanning was obtained (e.g. 3 x 3 grid) smaller operator matrices (i.e. 2 x 2, 2 x 3 and 3 x 2 spatial extent) were applied for the points around the central grid point. **Table III** illustrates the list of operators used for 3 x 3 grid measurements. For example, the directly observed power spectral peak values from multiple-point (3 x 3 points) measured alpha wave amplitudes were converted into a smooth data form. **Table IV** represents the original and smooth matrices for the 3 x 3 grid. The enhanced spectral values, in turn, could be displayed on the color monitor using a specially written computer graphic program. **Figure 20** shows the contour map representing the enhanced two-dimensional matrix of 3 x 3 grid measurements for simulated alpha-wave excitation.

7. Proof-of-Concept Prototype System

Optimization of fiber optic interferometric magnetometers for MCG/MEG applications has been accomplished by incorporation several innovative designs to the room temperature and portable instrument. These functions include: integrated assembly of the optoelectronic components into a single compact package; desired configuration of the first-order and the second-order gradiometer systems; and computer techniques for biomagnetic data processing, reduction and presentation. However, additional improvements are needed during the commercialization effort in Phase III of the program. For example, the complete brain wave characterization can be performed by combining both electric and magnetic recording in brain function studies (CHAPMAN et al., 1988). Thus, increased quantitative estimates of current dipole source localization is obtained. Such combined EEG/MEG measurements have been performed for interacranial localizations of the somatosensory cortex on patients (SUTHERLING et al., 1988). An ultra-sensitive instrument can be tested to measure simulated biomagnetic field signals as low as 10^{-14} Tesla. The MEG detects only the neuro-electrical sources in the brain which are oriented tangential to the skull, whereas the EEG detects both tangential and radial sources. Therefore, the MEG provides complimentary information to the EEG in localizing the current dipole sources in the brain. Such new information contained in the MEG appears to be useful in exactly locating diseased sources such as epileptic focuses.

Figure 21 illustrates the schematic of an instrument in which both electric and magnetic fields can be measured using a compact dual-sensing fiber interferometer. The interferometer contains two separate sensing fiber lines, one for magnetic field sensing attached to a magnetostrictive transducer and another for electric field sensing attached to a piezoelectric transducer. Only one reference arm

is used for both electric and magnetic fields. Alternative configurations in which magnetic and electric field sensors are attached together (e.g. in orthogonal arrangement) to form a multiple sensing probe could offer some advantages. In this design, each fiber is strained by both electric and magnetic fields. Compared with two separate electric and magnetic field sensor systems which require two laser sources, the hybrid design requires only a single laser source.

In regard to contact EEG transducers based on the flexible polymer piezoelectric fields, it is suggested that their potentially useful biomechanical properties be seriously exploited in EEG instrumentation. Although the EEG devices, in general, have good temporal resolution and excellent sensitivity, their spatial resolution is poor. For example, the multi-electrode scalp recordings of electrical potentials are modified by the different resistivities of the hard and soft tissues of the human brain. Such problems have been solved to some extent by the application of Laplacian spatial transformation of "deblurring" techniques which can improve the estimation of localization of EEG equivalent current dipole sources. However, the piezoelectric-based polymer/fiber optic interferometric instrument offers an alternative approach where the high lateral detection resolution is achieved by packaging new EEG multi-probes having lightweight and very small volumes. In addition, the hybrid combination of coupled EEG/MEG probes in the composite sensor head simultaneously provides a more realistic demonstration of electrical and magnetic activity measurements of the human physiological system. Consequently, the traditionally time consuming clinical testing and appointment schedules of such sophisticated EEG/MEG examinations is relaxed. Like the present EEG devices (COHEN, 1987) using multi-channel scalp electrodes, the flexible piezoelectric sensing elements of the improved neuromagnetic-electric sensing instrument come in contact with the head. Therein, the sensitive area of the probes lies along the contour surface of the head so that the component of the electric brain signal tangent to the surface is examined. The geometric positioning of this probe with respect to the MEG probe provides the optimal sensing configuration. This may result in an orthogonal sensor head arrangement as is depicted in Figure 21.

The detection of electric fields for EEG applications is similar to the approach taken for the magnetic sensing measurements except that a piezoelectric material (e.g., polymer PVDF) is mechanically coupled in the sensing fiber so that only EEG responses can be detected. The electric fields near the surface of the scalp mechanically excite the PVDF film due to the reciprocal piezoelectric effect which in turn optically modulates the bonded sensing fiber. The interferometric signal obtained from this special PVDF/fiber combination would directly correspond to the magnitude of neuro-electric fields. The probing laser beam is launched into a single-mode optical fiber coupler. One part travels through the undisturbed reference path while the other two travel through the sensing fibers subject to both electric and magnetic excitations. Two distinct interferometric signals can be simultaneously interrogated owing to the separate piezoelectric/magnetostrictive optical fiber responses.

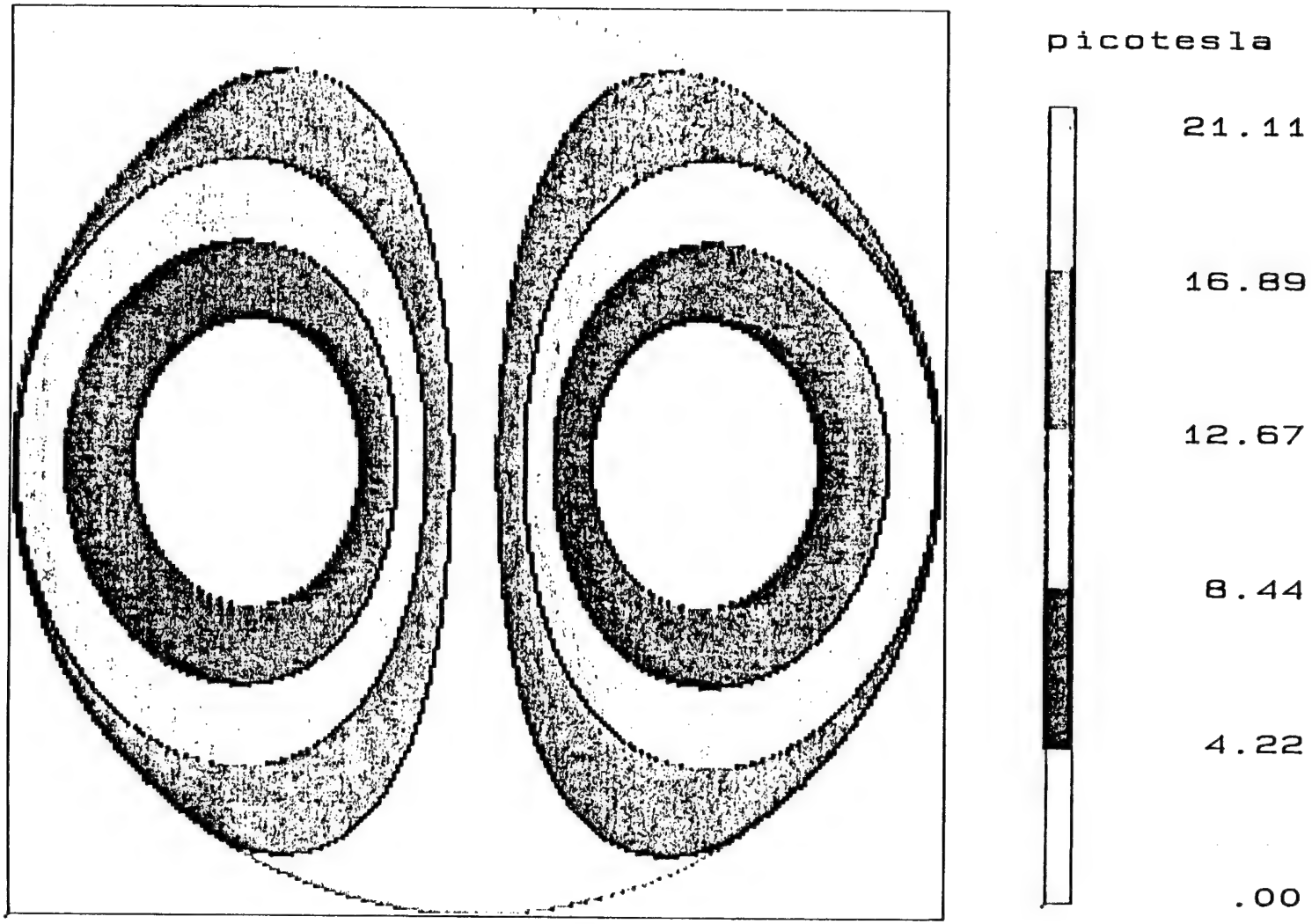

Figure 4. Magnetic Field Isocontour Maps for Radial Components of Brain Dipole Source.

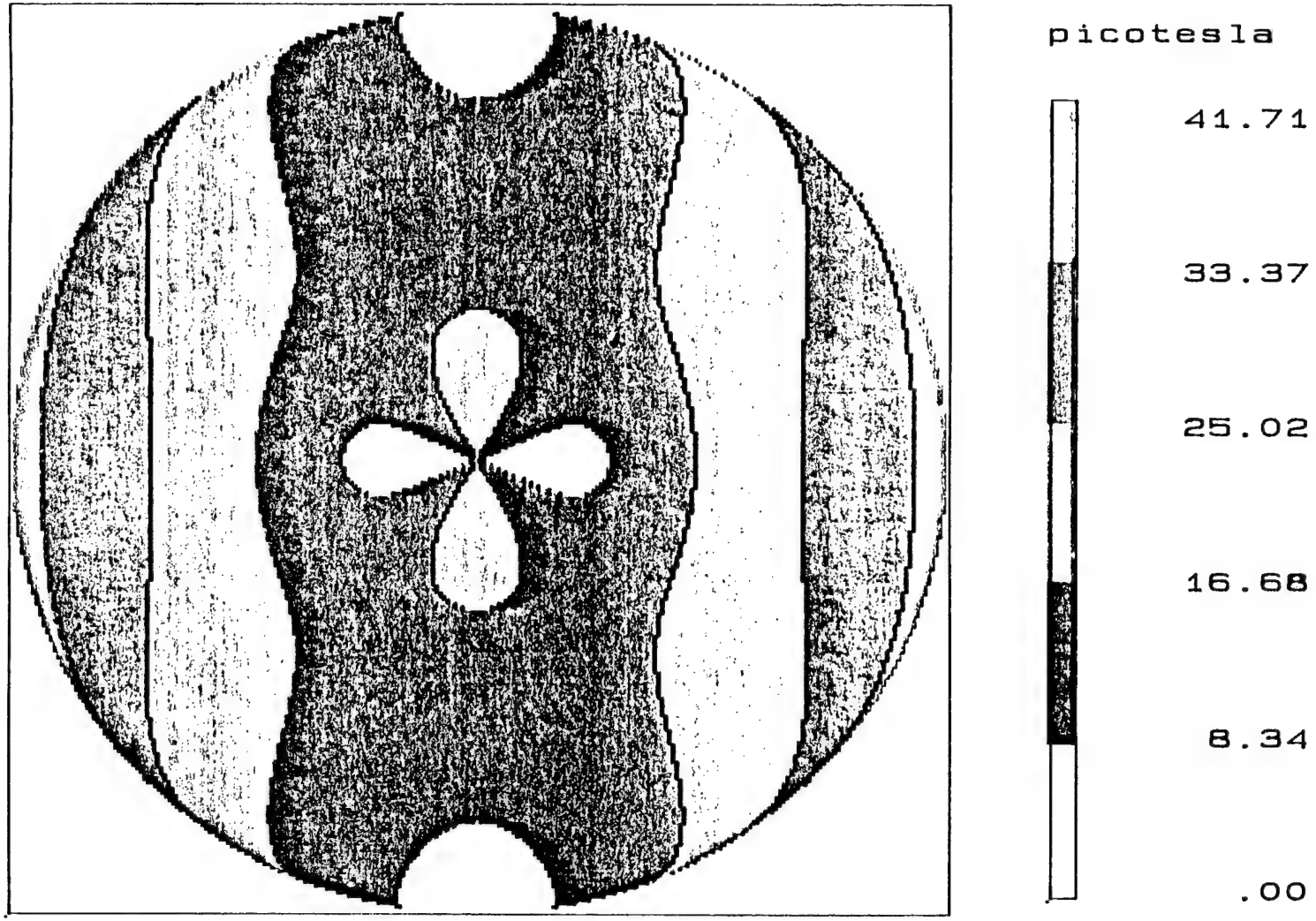

Figure 5. Magnetic Field Isocontour Maps for Tangential Components of Brain Dipole Source.

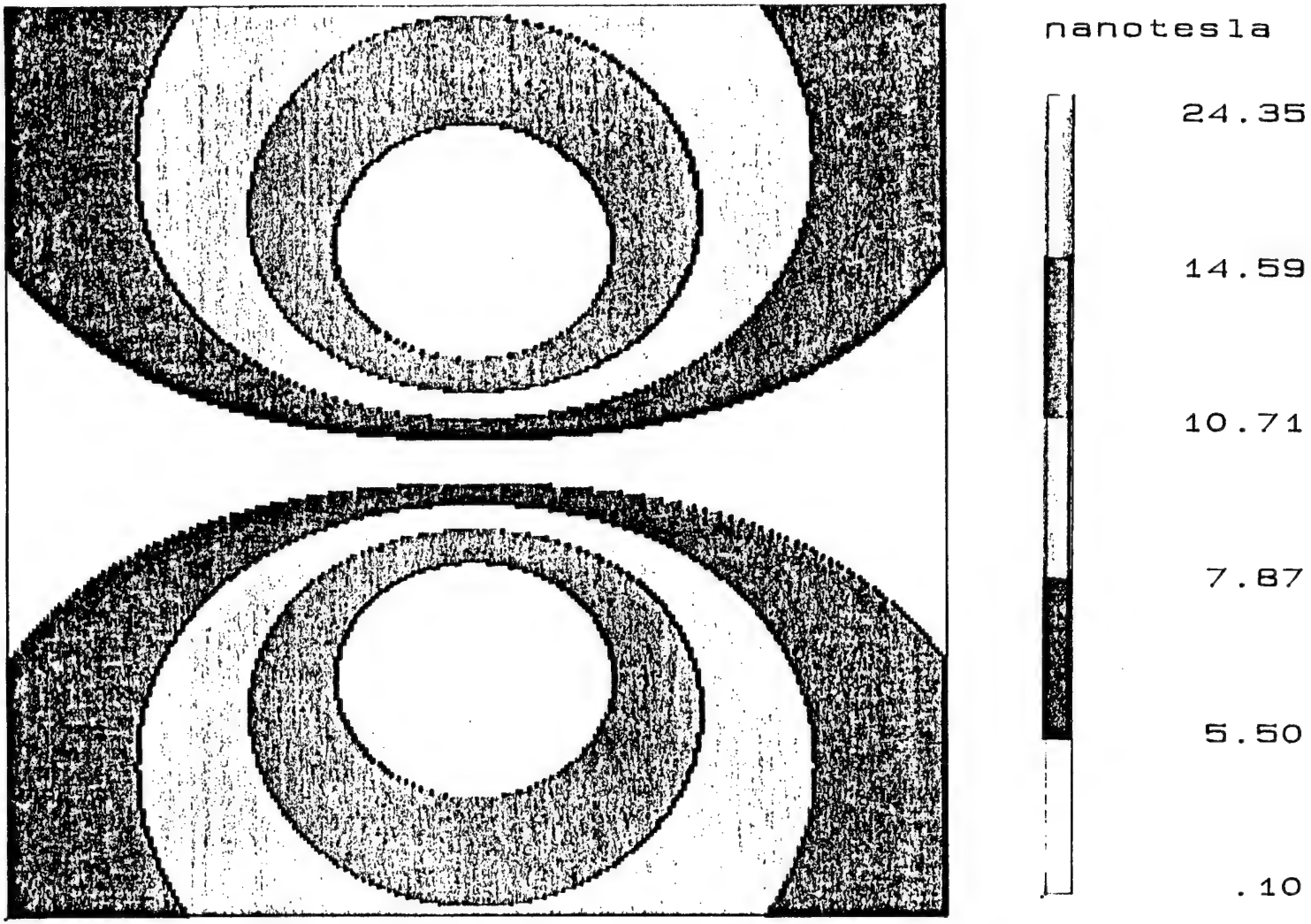

Figure 6. Magnetic Field Isocontour Maps for Radial Components of Heart Dipole Source.

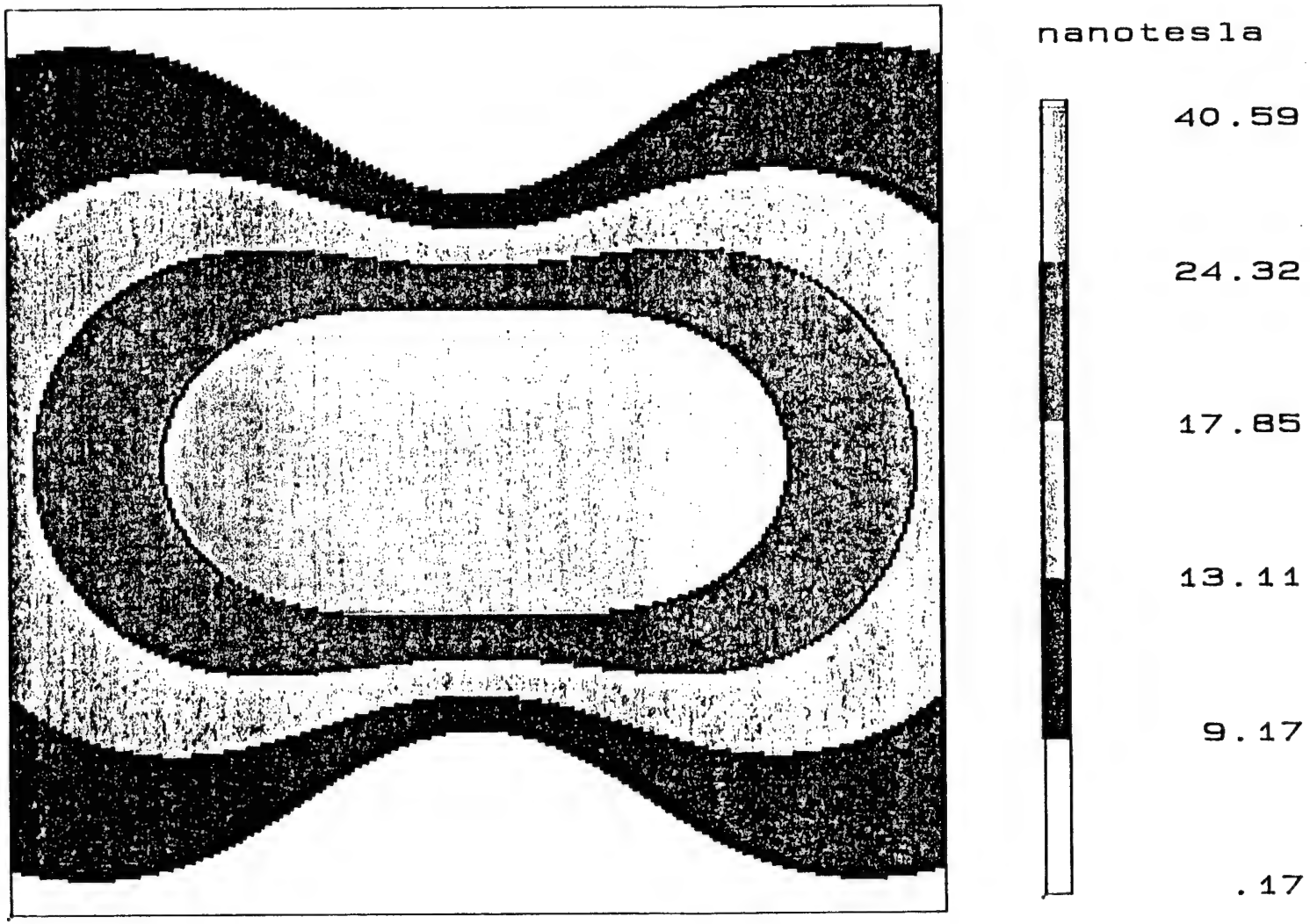

Figure 7. Magnetic Field Isocontour Maps for Tangential Components of Heart Dipole Source.

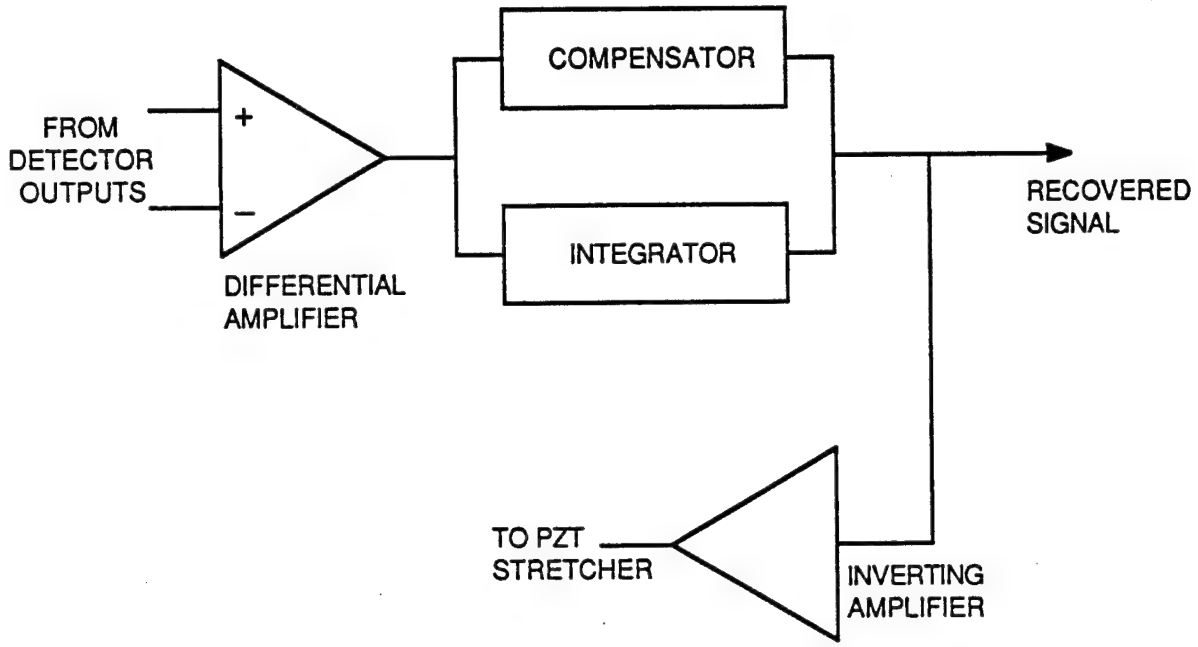

Figure 8. Schematic Diagram of Compensator System.

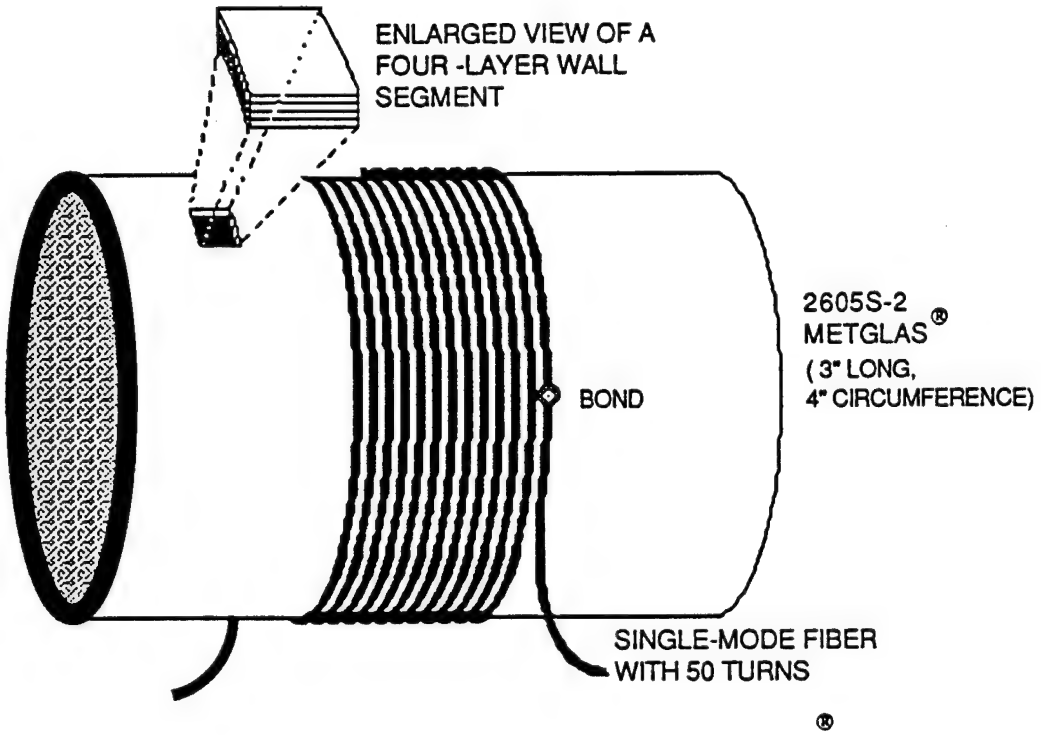

Figure 9. Schematic Illustration of Laboratory Constructed Metglas®/Optical Fiber Magnetic Field Sensor with Four-Layer Cylindrical Shell.

Table I. He-Ne Laser Based Compact Magnetometer Subcomponents

Item	Description
Lens	Intensity stabilized, 633 nm, 840 μW, Model 117A, Spectra-Physics
Micro Lens	SELFOC® GRIN Lens, 633 nm, 0.25 pitch, 2-mm diameter, 0.37 NA
Fiber Optic Positioner	Model FP-2 Newport Corporation
Single-Mode Fiber	633 nm, 4/125 core/cladding ratio, 0.1 NA, 12 dB/Km attenuation, Type F-SF, Newport Corporation
Fiber Couplers	633 nm, 50/coupling ratio, 122-129dB loss, Interfuse 945, Allied Amphenol Products
Magnetostrictive Material	Type 2605S-2, Metglas®, Allied Corporation
Piezoelectric Material	PZT-5H ceramic tube, Vernitron
Photodetector	Dual Element, UV-100 dual, EG & G Photon Devices
Q-Point Operating Unit	Servo Board, Model 911, Canadian Instrumentation & Research Limited

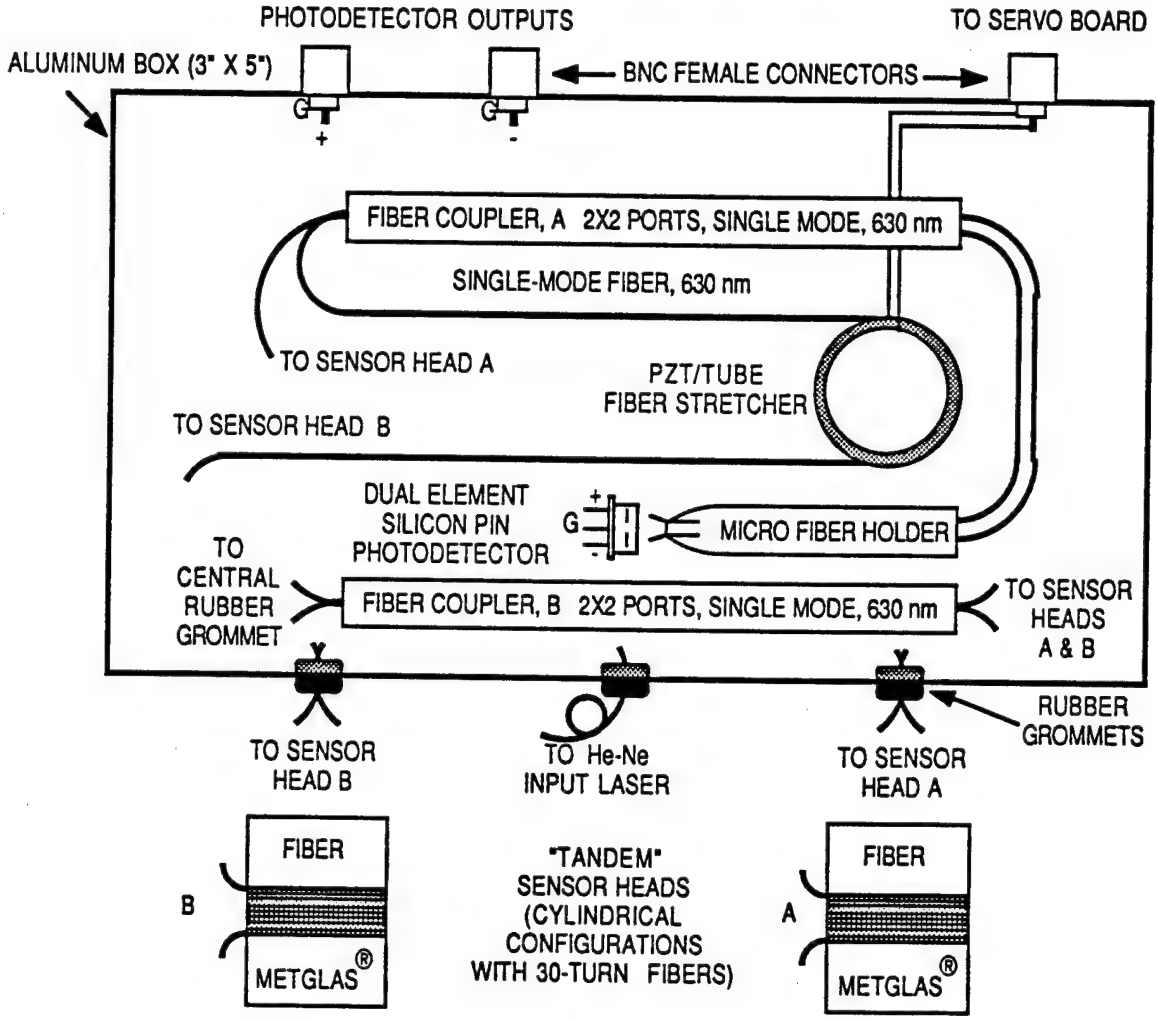

Figure 10. Optoelectronic Module Components of He-Ne Laser Magnetometer.

Table II. Laser Diode Based Compact Magnetometer Subcomponents

Item	Description
Laser Diode Power Supply	Stabilized, 300/600 mA, Canadian Instrumentation Research Limited
Semiconductor Laser Diode	Hitachi Laser Diode, Type HL 8312E, 810-850 nm lasing wavelength, ~ 10 mW power, Hitachi, Ltd.
Laser Diode Coupling Optics	Optimized at 0.85 μm, 90% transmission, Model 910, Canadian Instrumentation Research Limited
Single-Mode Fiber Couplers	2 x 2 ports, 830 nm operating wavelength, 0.10 - 0.18 dB excess loss, part no. T629-0830, ALCATEL
Fibers	Single-mode at 0.83 μm, 4.5/85 core/cladding ratio, 2.18 dB/km loss, 0.12 NA, Type T-1601, ITT Electro Optical Products Division
Photodetectors	Operational Amplifier/Photodiode combinations HUV-1100BG, EG&G

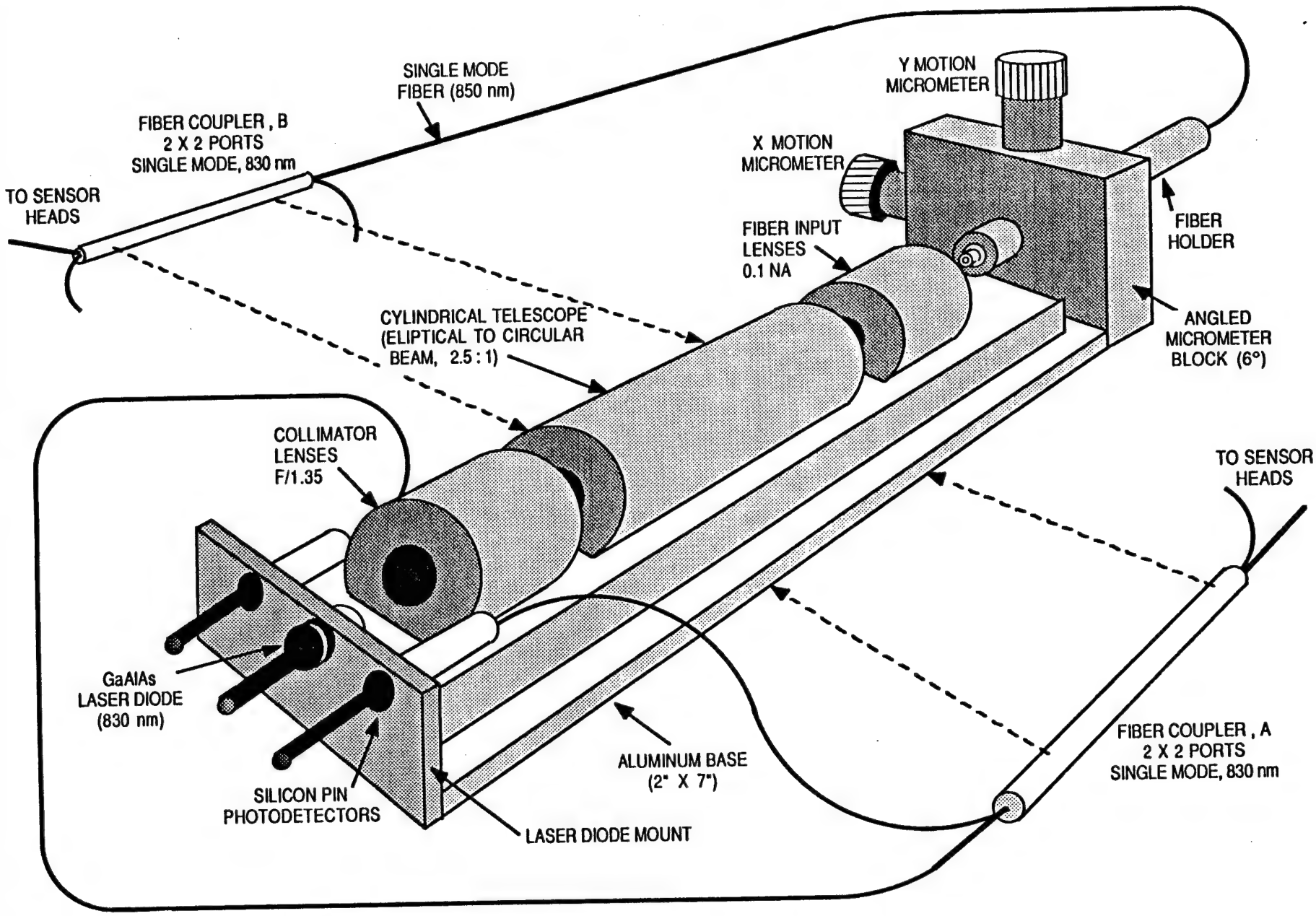

Figure 11. Perspective Illustration of Components for Laser-Diode Compact Magnetometer.

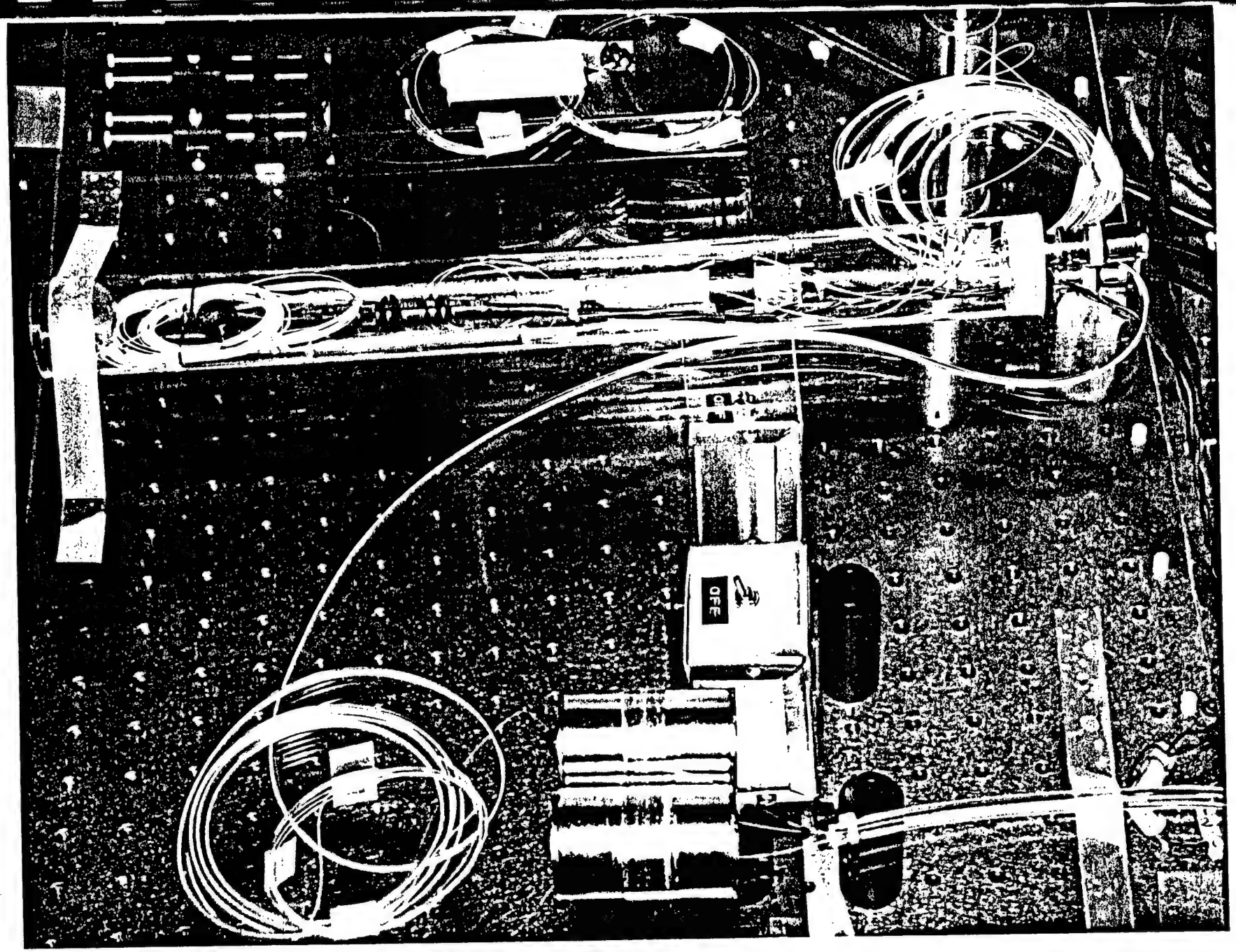

Figure 12. Subcompact Magnetometer.

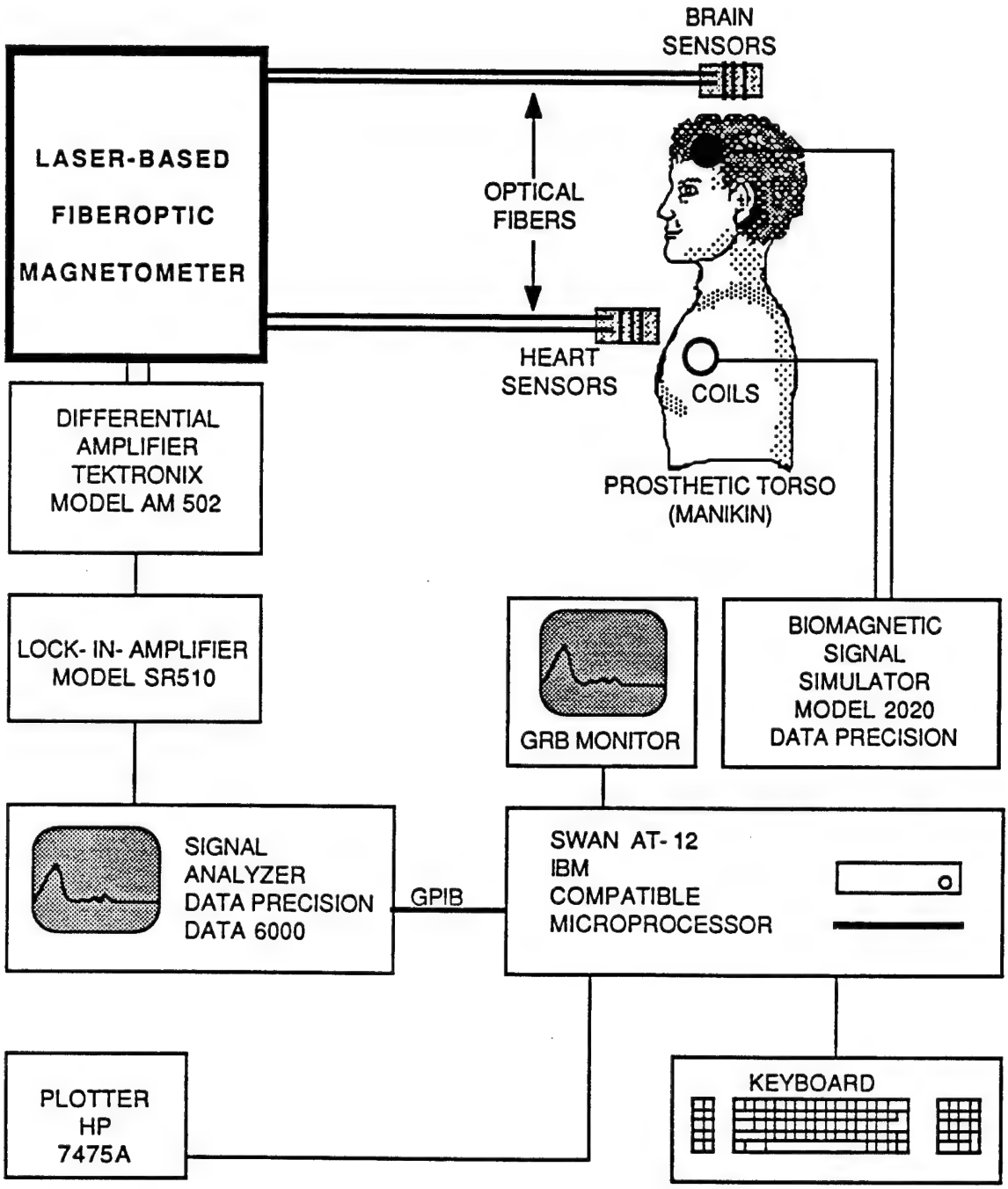

Figure 13. Experimental Arrangements of Fiber Optic Magnetometer Subsystems.

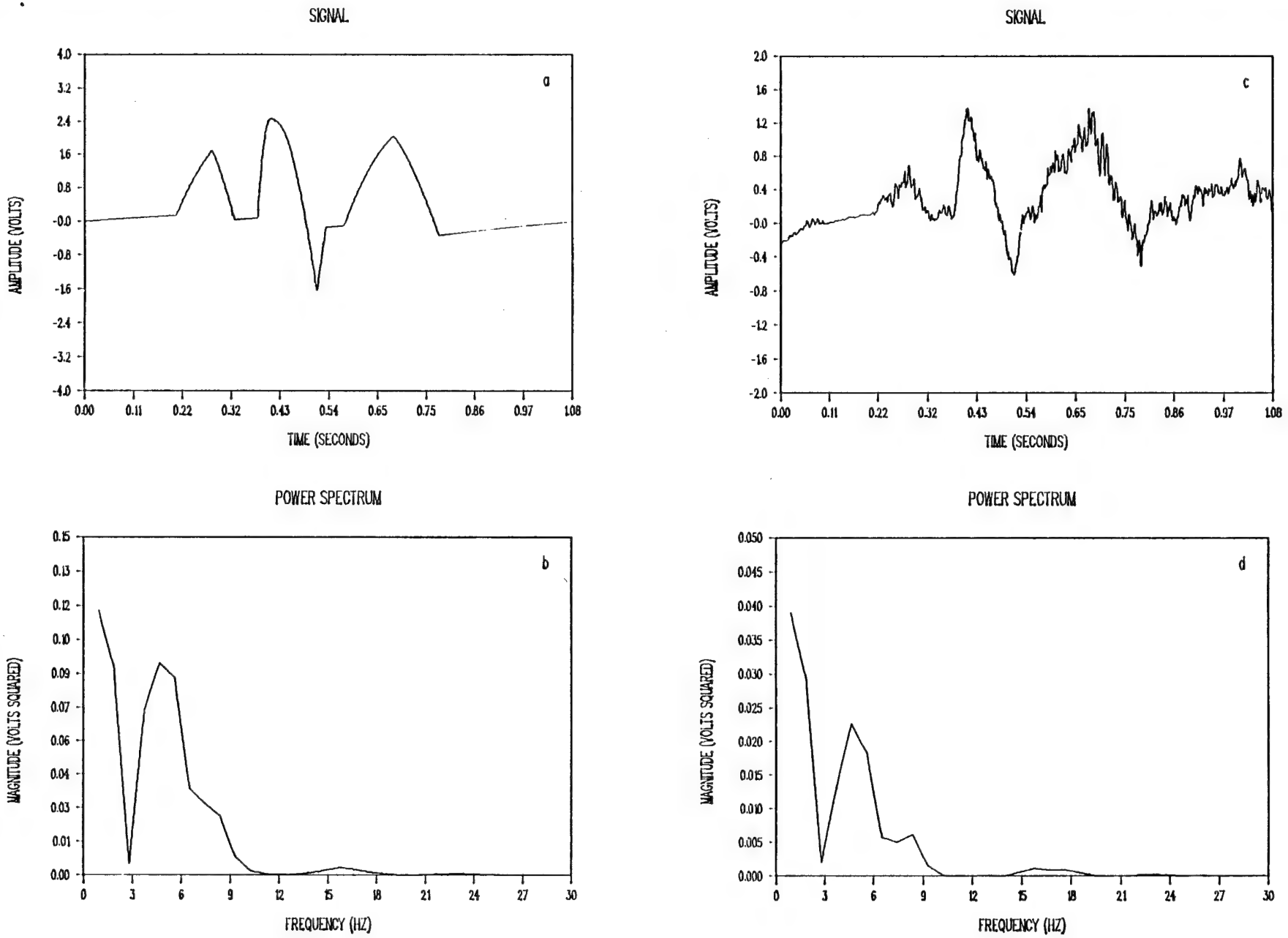

Figure 14. Waveforms and Spectra for Heart Signals: a and b, Input; c and d, Output.

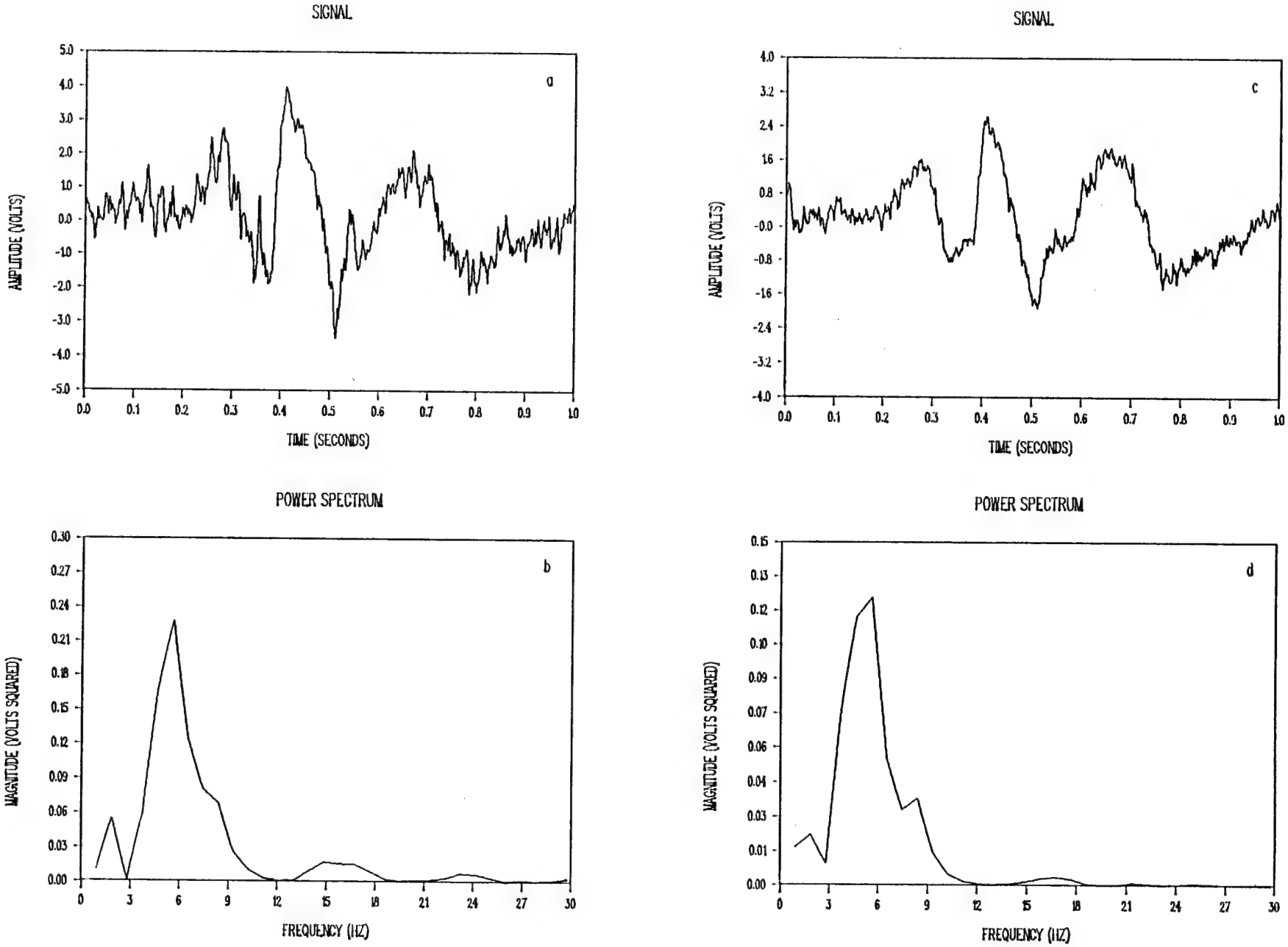

Figure 15. Waveforms and Spectra for Repeated Heart Outputs.

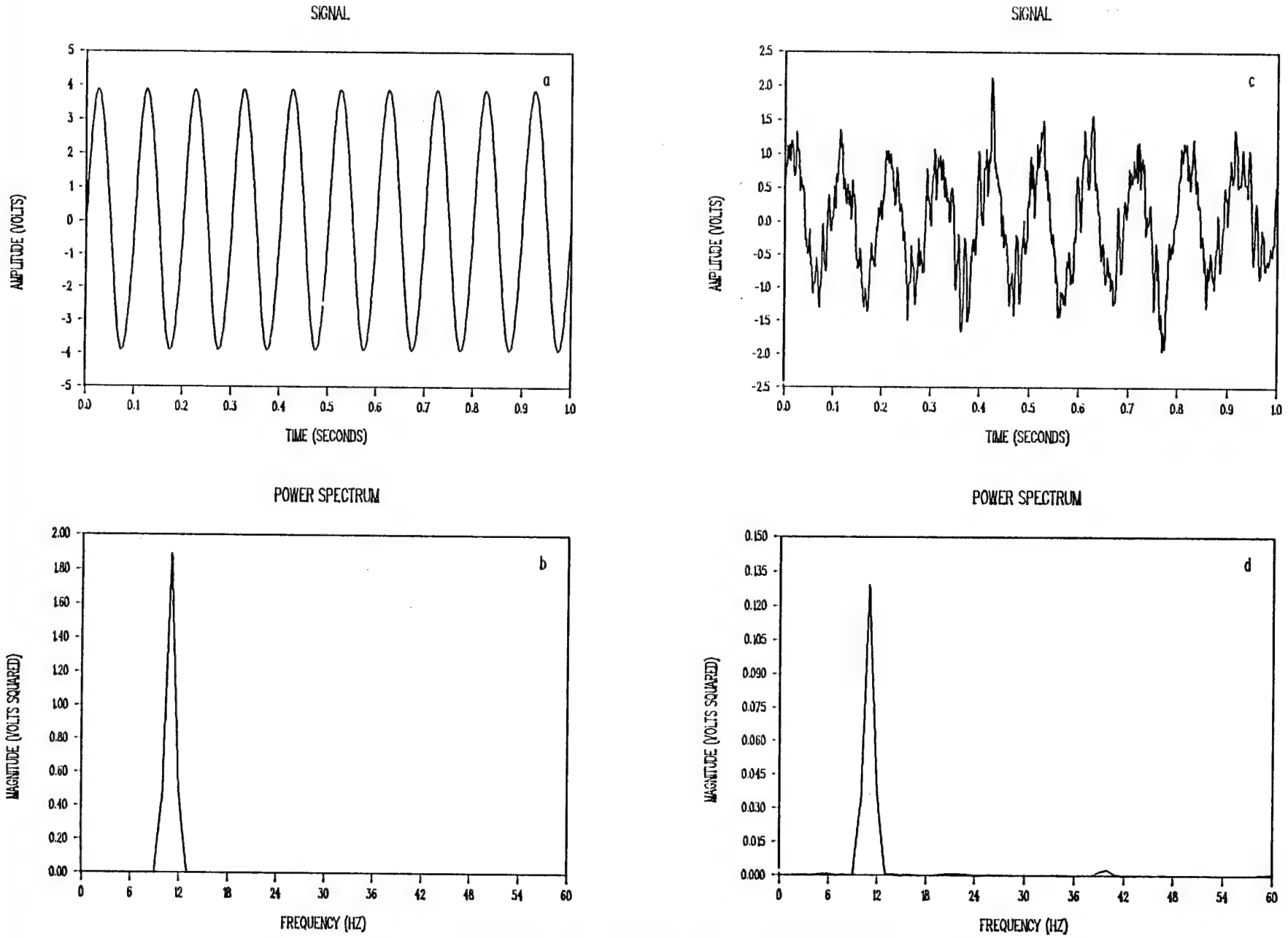

Figure 16. Waveforms and Spectra for Alpha Rhythm:
a and b, Input; c and d, Output Signals.

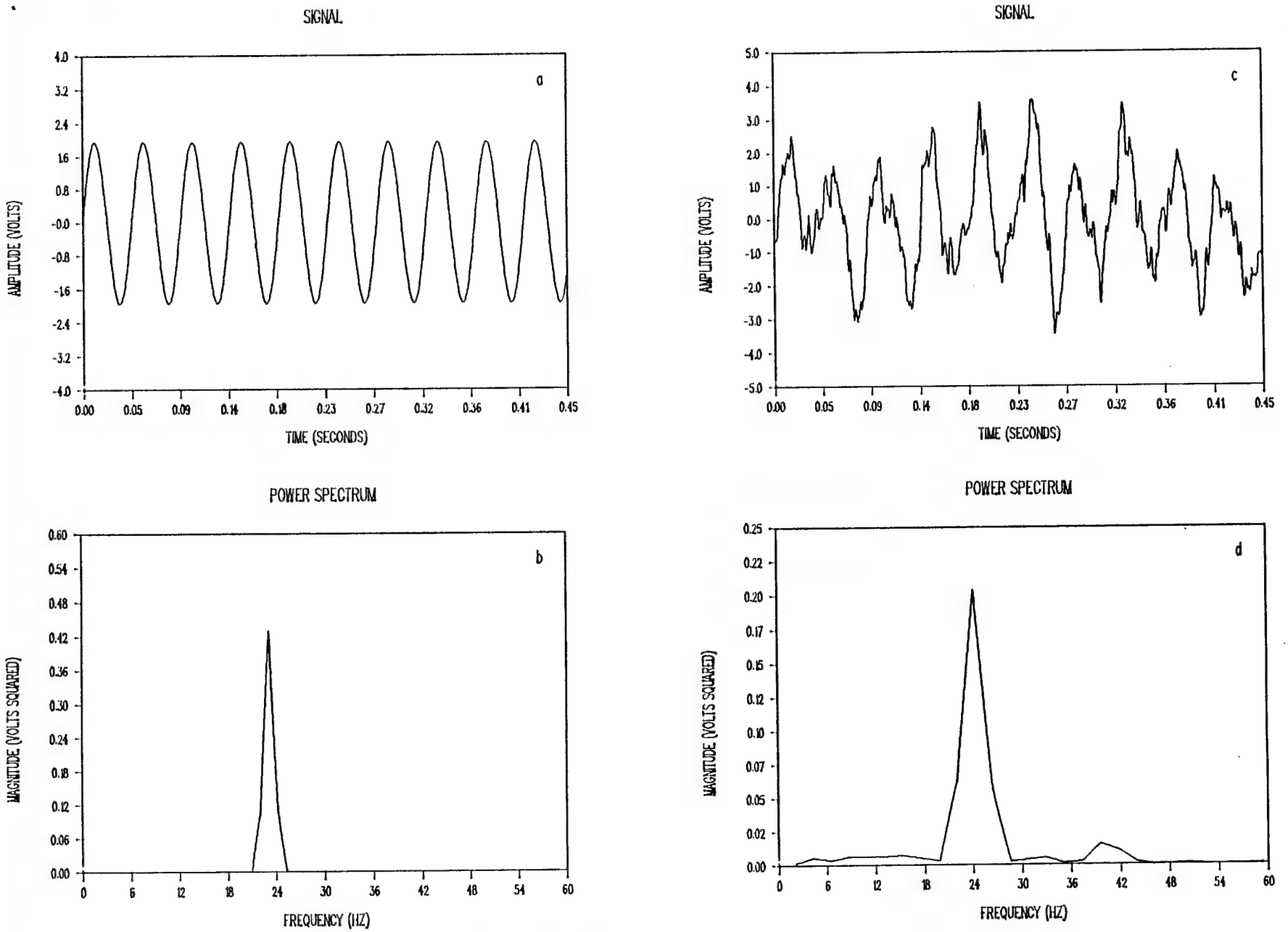

Figure 17. Waveforms and Spectra for Beta Rhythm: a and b, Input; c and d, Output Signals.

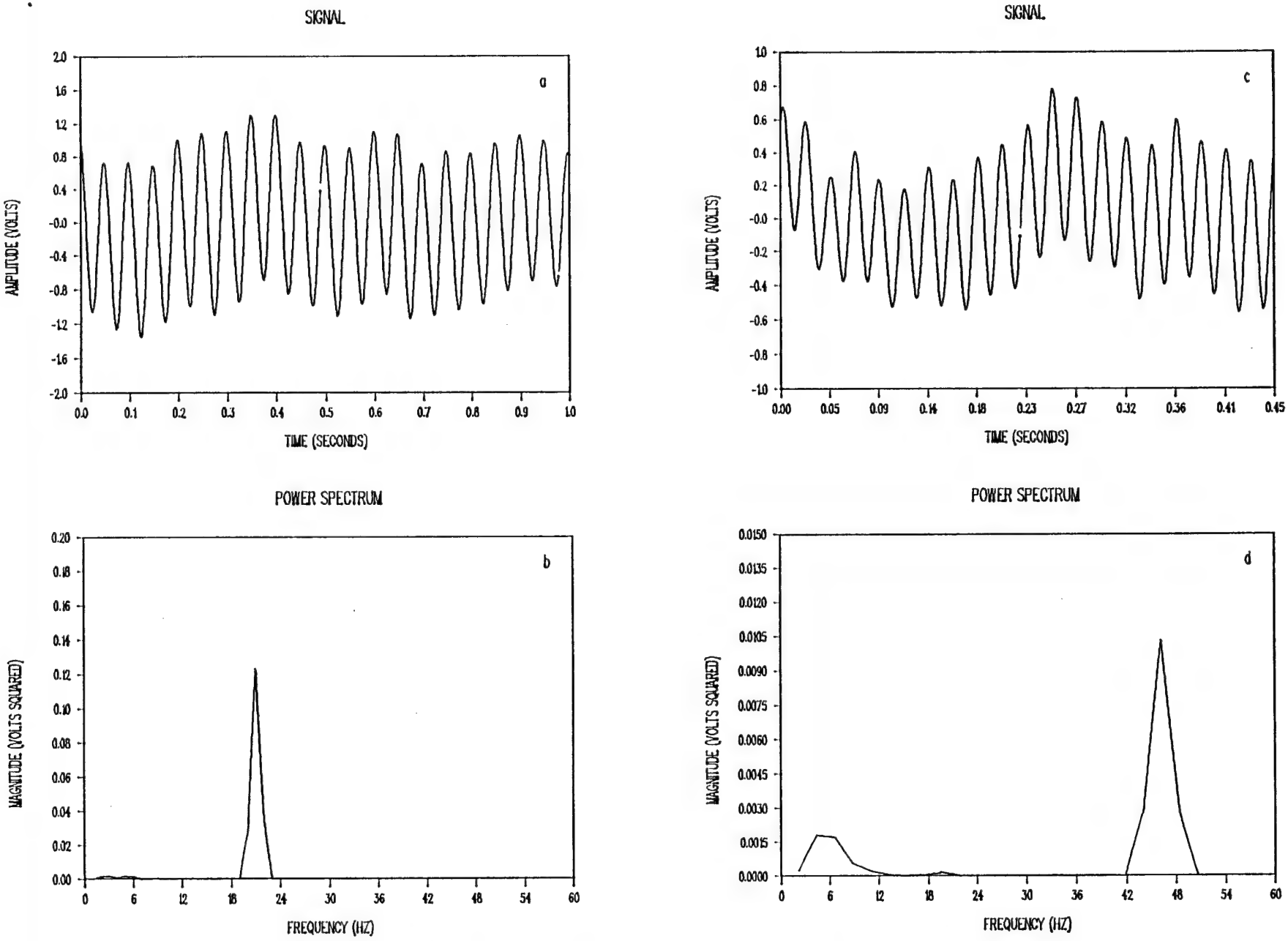

Figure 18. Waveforms and Spectra for Output Brain Waves Using Lock-in Amplification Technique.

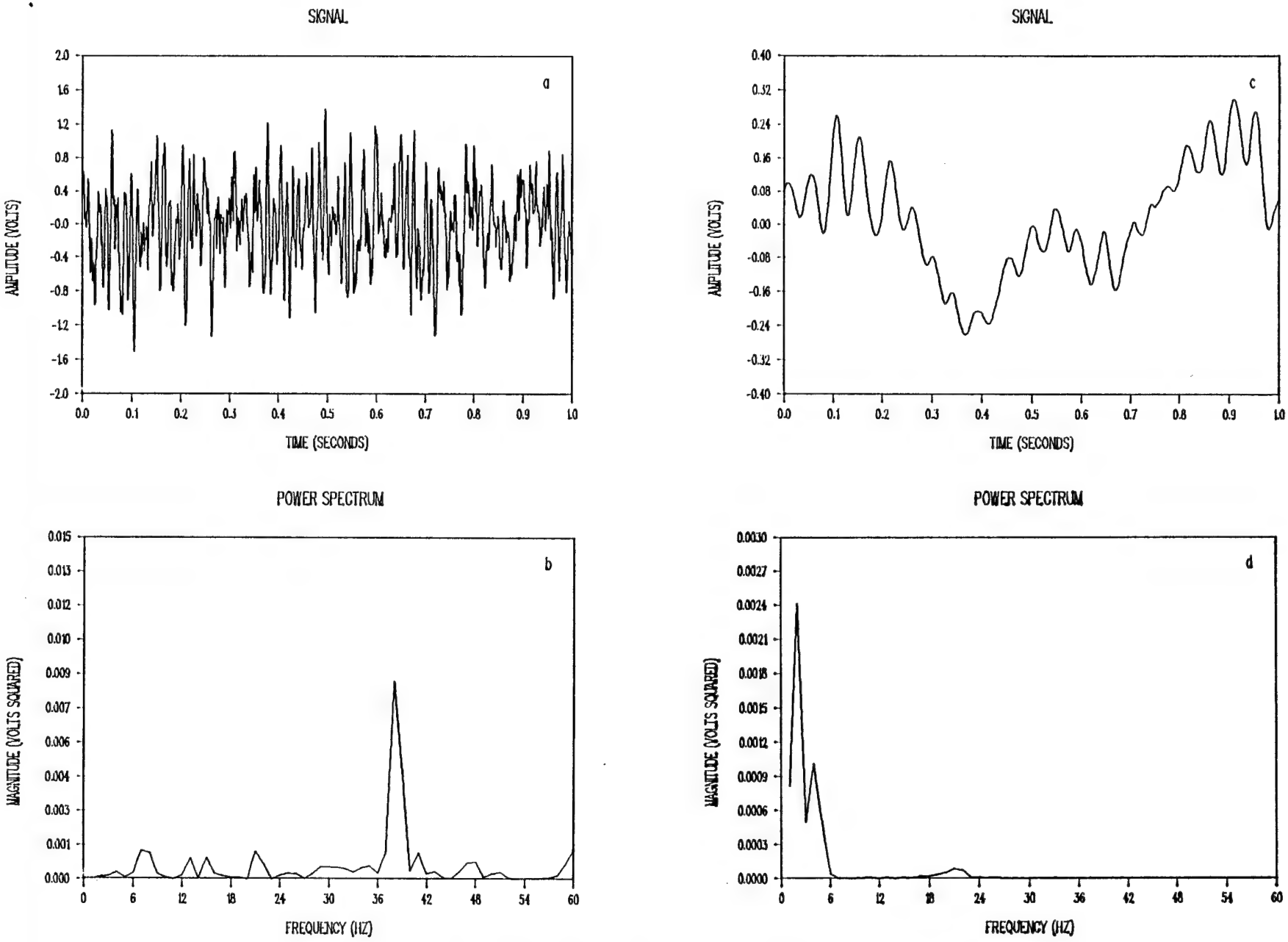

Figure 19. Waveforms and Spectra for Magnetometer System Noise: a and b, Differential Amplifier; c and d, Lock-in Amplifier.

Table III. Low Pass Filtering Operators for Each Point on 3 x 3 Grid.

4 2 2 1 9	2 4 2 1 2 1 12	2 4 1 2 9
2 1 4 2 2 1 12	1 2 1 2 4 2 1 2 1 16	1 2 2 4 1 2 12
2 1 4 2 9	1 2 1 2 4 2 12	1 2 2 4 9

Table IV. Application of Digital Averaging Technique.

	Original			Smooth		
power spectral peaks ($\mu v^{**}2$)	36.2	13.5	142.0	79.8	115.7	119.3
	40.0	466.0	6.1	122.4	149.2	110.4
	123.0	45.4	13.0	125.4	119.3	69.0

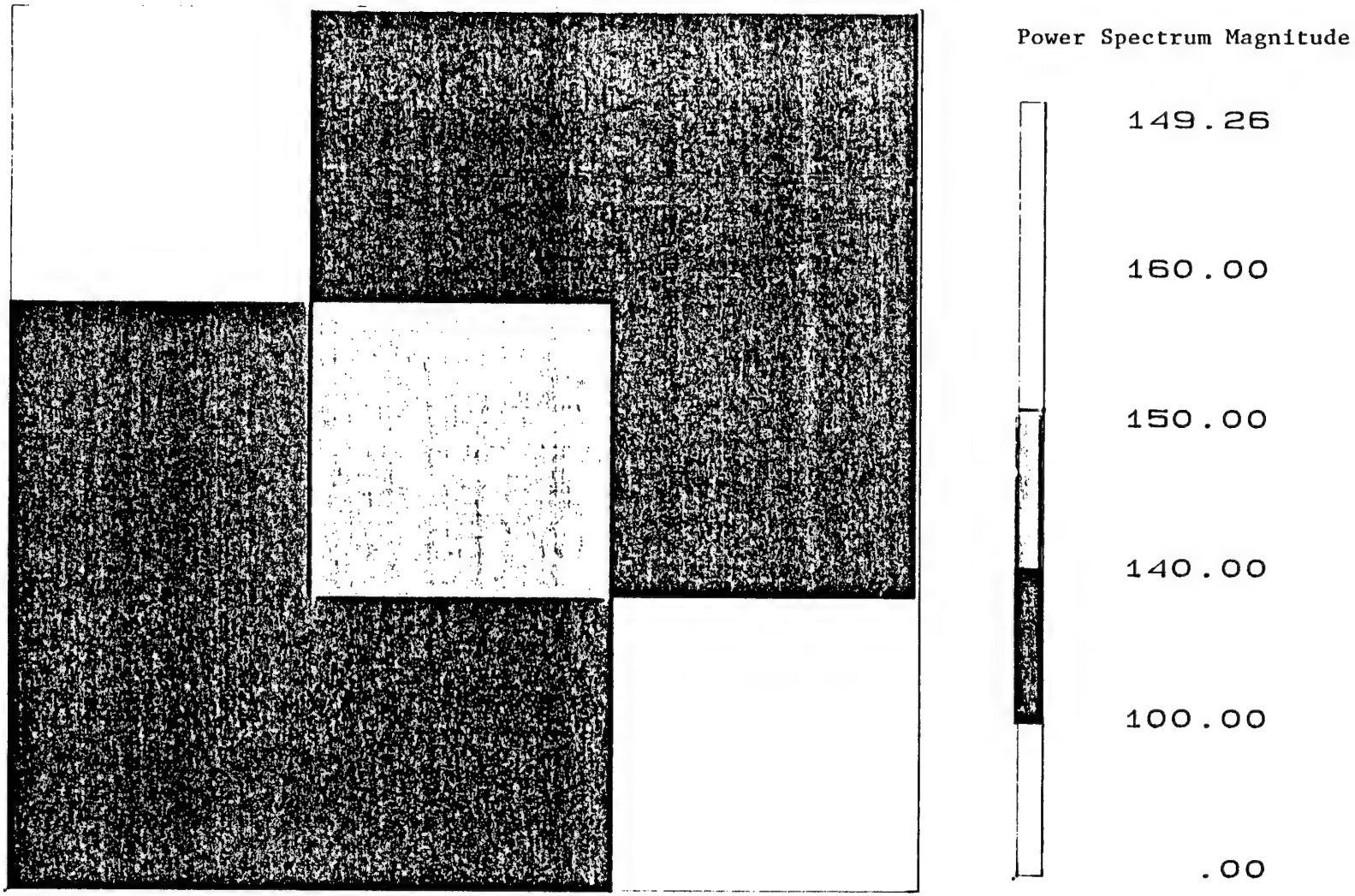

Figure 20. Contour Map of Measured and Specially Enhanced Spectral Peaks for 3 x 3 Grid Points.

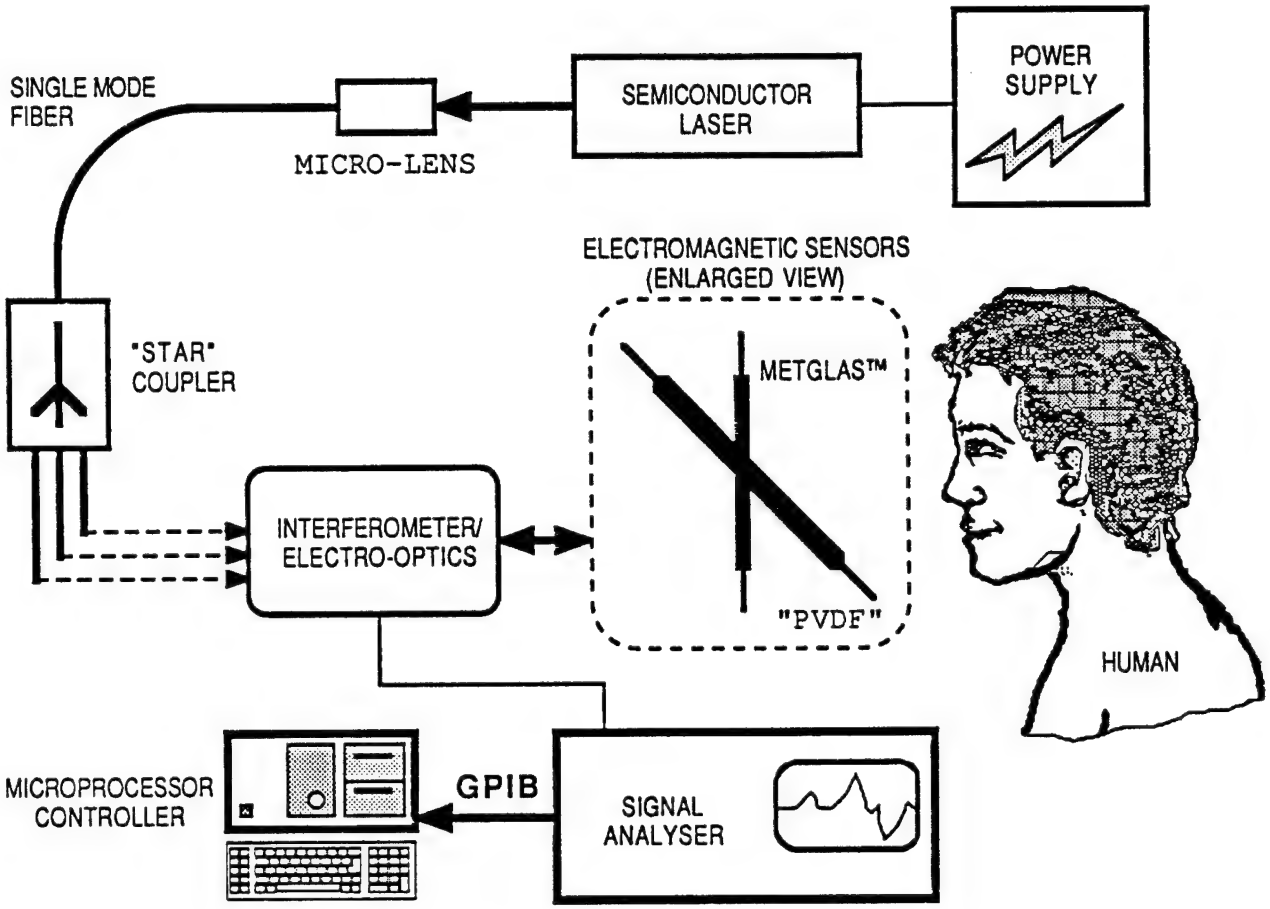

Figure 21. Conceptual Design of Instrument for Human Magneto-electrophysiological Measurements.

VII. CONCLUSIONS AND POTENTIAL APPLICATIONS

The research program evaluated the performance characteristics of economically inexpensive instruments based on fiber optic interferometry and magnetostriction effects for human biomagnetic field measurements. The following sections briefly summarize the work, describe the accomplishments and highlight the potential commercial applications.

1. Conclusions

The research work undertaken in "laser fiber optic sensor for human biomagnetic measurements" should open new windows on the study of the brain, heart and other organs. The inherent advantages of noncontacting, compact, room temperature biomagnetic fiber optic sensors with respect to existing SQUIDs could lend greater flexibility in magnetophysiology and biomedical applications. For example, the combined utilization of fiber optic biomagnetic field sensing technology and desktop computer incorporated in this project could help needed developments in vision research, imaging techniques, magnetophysiology and neural science. The prototype instrument described in detail in the previous technical reports has the desired performance needed to make MCG measurements. Specifically, simulated biomagnetic field measurements have resulted in minimum detectable magnetic fields of about 10 picoTesla. Alternative designs of gradiometers such as first-order and second-order configurations have been incorporated. For future development to be carried out in the Phase III program, the signal-to-noise ratio would be enhanced by combination of several noise reducing mechanisms, that is, both passive and active designs including shielding, filtering and post processing techniques are used. The presently available single-channel device would be modified to a multiple-channel sensor by increasing the number of optical fiber couplers and hybrid sensor heads. Finally, the sensor head of prototype fiber optic interferometer magnetometer can be miniaturized using special optical waveguide operations based on the magneto-optical characteristics of nonmetallic crystal materials. The market niche for application of fiber optic electromagnetic sensors already exists, and significant growth in the area of biomedicine is expected over the next six years.

2. Accomplishment of Phase II Objectives

The Phase II project dealt with construction and testing of several compact magnetometers for eventual medical and aerospace applications. Major research areas investigated during the previous reporting periods include computer modeling of human magnetocardiographic and magnetoencephalographic fields, evaluation of active homodyne laser interferometers in the proposed fiber optic magnetometers, and experimental demonstration of several compact fiber optic magnetometers in simulated magnetocardiology (MCG) and magnetoencephalography (MEG) within an instrumented prosthetic manikin. The Phase II research effort constituted the investigation of the following technical

objectives: extension of magnetostrictive/fiber interaction models; improvement of the fiber optic interferometer design; evaluation of methods to increase the magnetostriction-to-fiber strain transfer efficiency; integration of hybrid micro-optoelectronic magnetometers; application of multiple layer sensor arrays and gradiometer operation; acquisition of families of simulated biomagnetic test data; and optimization of a proof-of-concept system.

Specific features and performance capabilities of the laboratory prototype magnetometers are summarized as follows:

- Compact and portable design having the ability of room-temperature operation.
- Integration with an instrumented manikin for simulated MCG/MEG demonstration as a research tool.
- Computer-aided graphic capabilities for presentation and display of biomagnetic field measurement data.
- Presently achieved instrument response characteristics of greater than 80 decibels (signal-to-noise ratio) resulting to 10 picoTesla (rms) noise level.

Phase II research in developing interferometric fiber optic magnetometers has provided encouraging results concerning the application of such noncontacting techniques for biomagnetic measurements including magnetophysiology and/or neuro-cardiac disease diagnostics. Considerable effort has already been made in demonstrating the performance characteristics of the prototype magnetometers. Simulation measurements were obtained in both the laboratory and the medical research facilities. For example, the performance capabilities of the Phase II program were demonstrated in front of a team of medical doctors at a medical research hospital (Charlotte Memorial Hospital and Medical Center, Electro-Physiology Laboratory). It is expected that advanced system development of the sensor to be achieved in Phase III program will make it a rugged field usable instrument. Such a complete system will contain a series of multiple channel sensors for precise dipole localization and mapping purposes. The additional optimization in the interferometric magnetometer configurations should improve the magnetic field detection sensitivity so that the very weak brain signals can readily be recorded. The Air Force should benefit from a small biomagnetic sensor that permits continuous monitoring of the physiological conditions of flight personnel such as fighter pilots during combat flight and high-g maneuvers. The real-time MCG/MEG measurements may provide the precursor signals due to the unconsciousness and indicate the pilot workload, overload, stress and blackout. The miniaturized sensor heads would be embedded into a flight helmet or vest and be used in normal cockpit environments. ARCOVA is aggressively pursuing the future market and extension of the present technology for both the military and civilian applications.

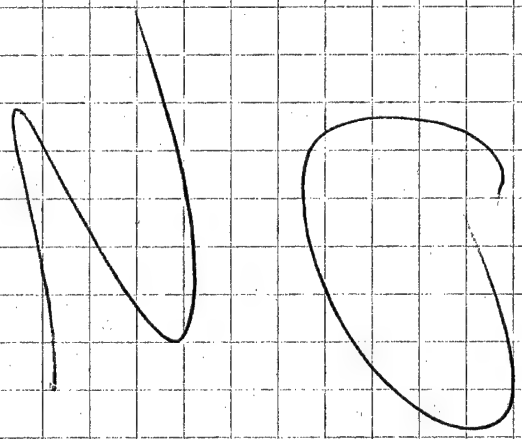

page

62

At higher frequencies, the fiber optic magnetometer could be used for the detection of very low frequency electromagnetic waves (EDWARDS, 1984). Such sensors can be used in remote sensing and remote monitoring applications. It is known that the fiber optic magnetometer can operate at frequencies over 1000 Hz in a standard configuration with 100,000 Hz feasible for coated fibers.

The fiber optic magnetometer could also find commercial application in geo-exploration where the large fiber length per unit volume could be used to investigate subsurface geological deposits having differing magnetic signatures from surrounding strata. The feasibility of fiber optic detection of very low frequency radiation could be used for subsurface exploration as well as undersea communications.

Many of the advances suggested by this proposal in achieving the highly sensitive fiber magnetometer could find commercial and military applications. The methods investigated for increasing the strain coupling between a magnetostrictive material and an optical fiber could be employed in fiber optic piezoelectric sensors. Similarly, the techniques for fiber optic multiplexing suggested in this proposal could be useful in communications and nondestructive testing applications. At present, there is a need for devices capable of digitizing transducer output and sending that digitized output through a noisy environment. This need can be met through equipment designed for the signal analysis of the fiber optic magnetometer. Finally, the magnetometer array could be used for robot tactile sensing and robot vision. In robot tactile sensing of ferromagnetic materials, the fiber magnetometer array can provide information on the proximity of the portion of the robot hand to the object as well as the strain induced in the object through inverse magnetostrictive techniques. In robot vision, the fiber array developed in this program could be used for scanning during robot operations.

The American Research Corporation of Virginia has obtained a Follow-on Funding Commitment from a venture capital group for a portion of the Phase III commercialization aspects of the program. Discussions and negotiations are currently underway with several industrial companies for the remaining applications identified in the Phase II effort.

VIII. ACKNOWLEDGEMENTS AND DISSEMINATION OF INFORMATION

1. Acknowledgements

This work was supported by the U.S. Air Force, Armstrong Aerospace Medical Research Laboratory, Human Systems Division, Wright-Patterson Air Force Base under SBIR Phase II Contract No. F33615-87-C-0546. Dr. Glenn F. Wilson, Technical Monitor, is greatly appreciated for his encouragements during the course of the program.

Principal Investigator, R. J. Churchill, and Associate Investigator, A. Sarrafzadeh, wish to acknowledge the technical contribution of the subcontractor (under the direction of Dr. R. O. Claus) at Fiber and Electro-Optics Research Center, Virginia Polytechnic Institute and State University. The authors would also like to thank R&D staff, associates and colleagues for their assistance on various phases of the program: Dr. U. V. Vaseashta, Dr. M. G. Niimura, Ms. G. B. Churchill and Mr. D. L. Whitman. Special gratitude is also offered to Dr. S. P. Almeida for his consulting on biomedical applications.

2. Dissemination of Information

No formal presentation or publications of the results of this Phase II program were made outside the Air Force (Dr. Glenn F. Wilson, Armstrong Aerospace Medical Research Laboratory, Human Systems Division, Wright-Patterson AFB, Ohio 45433-6573).

During the course of the program it was necessary to brief the consultants to the program on the results of certain of the experimental evaluations performed. Consequently, some of the data acquired during the Phase II program has been disseminated to Dr. S. P. Almeida, Department of Physics, University of North Carolina at Charlotte. In addition, the performance capabilities of the Phase II program were demonstrated in front of a team of medical doctors at a medical research hospital (Charlotte Memorial Hospital and Medical Center, Electro-Physiology Laboratory).

IX. REFERENCES

Aittoniemi, K., Katila, T., Kussela, M-L. and Varpula, T. (1979), "Magnetoretinography: Detection of the Transient Magnetic Field of the Eye," Proceedings of the 12th International Conference on Medical and Biological Engineering, Jerusalem, ch. 96.4.

Baule, G. M. and McFee, R. (1963), "Detection of Magnetic Field of the Heart," American Heart Journal, vol. 66, pp. 95-96.

Beatty, J., Barth, D. S., Richer, F. and Johnson, R. A. (1986), "Neuromagnetometry," Psychophysiology: Systems, Processes and Applications, edited by M. Coles, E. Donchin, and S. Porges, The Guilford Press, New York, pp. 26-40.

Brenner, D., Williamson, S. J. and Kaufman, L. (1975), "Visually Evoked Magnetic Fields of the Human Brain," Science, vol. 190, pp. 480-82.

Chapman, P.M., Modena, I., Narii, L., Pizzella, V., Romani, G.L. et al. (1988), "Electric and Magnetic Brain Activity Related to Cognitive Performance," AGARD Conference Proceedings, No. 432, paper No. 10.

Churchill, R.J., Sarrafzadeh, A., Groger, H.P. and Churchill, G.B. (1987), "Laser Fiber Optic Sensor for Human Biomagnetic Measurements," AF SBIR Phase I Final Report, Contract No. F33615-86-C-0548.

Cohen, D. (1969), "Detection and Analysis of Magnetic Fields Produced by Bioelectric Currents in Humans," Journal of Applied Physics, vol. 40, pp. 1046-48.

Cohen, D. (1972), "Magnetoencephalography: Detection of the Brain's Electrical Activity With a Superconducting Magnetometer," Science, vol. 175, pp. 664–66.

Cohen, D. and Givler (1969), "Magnetomyography: Magnetic Fields Around the Human Body Produced by Skeletal Muscles," Applied Physics Letters, vol. 21, pp. 114-16.

Cohen, D., Edelsack, E. A. and Zimmerman, J. E. (1970), "Magnetocardiograms Taken Inside a Shielded Room with a Superconducting Point Contact Magnetometer," Applied Physics Letters, vol. 16, pp. 278-80.

Cohen, D., Palti, Y., Cuffin, B. N. and Schmid, S. J. (1980), "Magnetic Fields Produced by Steady Currents in the Body," Proceedings of the National Academy of Sciences, USA, vol. 77, pp. 1447-51.

Cohen, J. (1988), "Electroencephalography," McGraw-Hill Encyclopedia of Science and Technology, vol. 9, pp. 706-8.

Cuffin, B.N., and Cohen, D. (1977), "Magnetic Fields of a Dipole in Special Volume Conductor Shapes," IEEE Transactions on Biomedical Engr., Vol. BME-24, No. 4.

Dandridge, A. and Miles, R. O. (1983), "Laser Noise in Fiber Optic Interferometer Sensors," in Fiber Optics '83, pp. 165-70.

Dandridge, A. and Tveten, A. B. (1981), "Noise Reduction in Fiber Optic Interferometer Systems," Applied Optics, vol. 20, pp. 2337-39.

Dandridge, A., Tveten, A. B., Koo, K. P. and Giallorenzi, T. G. (1983), "Demodulation Schemes for Fiber Optic Sensors," in Fiber Optics '83, pp. 202-05.

Duncan, B.D., Weincko, J.A., and Claus, R.O., "Fiber Optic Magnetic Field Sensors Employing Metallic Glass Ribbons," Fiber and Electro-Optics Research Center, Virginia Tech, Subcontract Report to ARCOVA, 1988

Edwards, R. B. (1984), "Research Study of Fiber Optic Interferometry at Very Low Frequencies," TRW Report 43407.00 Contract N00019-83-C-0382.

Hughes, J. R., Cohen, J., Maynan, C. I., Scholl, M. L and Hendrix, D. E. (1977), "Relationship of the Magnetoencephalogram to Abnormal Activity in the Electroencephalogram," Journal of Neurology, vol. 217, pp. 79-93.

Hukkinen, K., Kariniemi, V., Katila, T. E., Laine, H., Lukander, R. and Makipaa, P. (1976), "Instantaneous Fetal Heart Rate Monitoring by Electromagnetic Methods," American Journal of Obstetrics and Gynecology, vol. 125, pp. 1115-20.

Jackson, D. A., Priest, R., Dandridge, A. and Tveten, A. B. (1980), "Elimination of Drift in a Single Mode Optical Fiber Interferometer Using Piezoelectrically Stretched Coiled Fiber," Applied Optics, vol. 19, pp. 2926-29.

Karp, P. J., Katila, T., Makipaa, P. and Saar, P. (1976), Proceedings of the 11th International Conference on Medical and Biological Engineering, Ottawa, pp. 504-5.

Lagakos, N. and Bucaro, J. A. (1981), "Minimizing Temperature Sensitivity of Optical Fibers," Applied Optics, vol. 20, no. 19, October, pp. 3276-78.

Livingston, J.D. (1982), "Magnetomechanical Properties of Amorphous Metals," Physica Status Solidi, vol. 70, pp. 591-96.

MacAulay, C. E., Stroink, G. and Horacek, B. M. (1985), "Signal Analysis of Magnetocardiograms and Electrocardiograms to Test Their Independance," Biomagnetism Applications and Theory, edited by H. Wenberg, G. Stroink and T. Katila, Pergammon Press, pp. 115-20.

Mizutani, Y. and Kuriki, S. (1986), "Somatically Evoked Magnetic Fields in the Vicinity of the Neck," IEEE Transactions on Biomedical Engineering, vol. BME-33, no. 5, pp. 510-15.

Nader, N., Ramchander, R., Wiencko, Jr., J.A., Poon, T.C. and Clans, R. O. (1990), "Fiber Optics Sensor and Device Research," Subcontractor Final Report, Fiber and Electro-Optics Research Center, Virginia Tech.

Romani, G. L., Williamson, S. J. and Kaufman, L. (1982), "Biomagnetic Instrumentation," Review of Scientific Instrumentation, vol. 53, no. 12, pp. 1816–45.

Sams, M., Hari, R., Kaukaranta, E., Reinikainen, K., Alho, K., Hamalamen, M. S., Ilmoniemi, R. J., Naatanen, R. and Salminen, J. (1985), "Magnetic Responses to Pitch Changes in a Sequence of Short Auditory Stimuli," Biomagnetism: Applications and Theory, Pergamon Press, New York, pp. 331-35.

Sudeora, S., "Laser FO Sensor for Human Biomagnetic Measurements," Fiber and Electro-Optics Research Center, Virginia Tech, Subcontract Report to ARCOVA, 1988

Sutherling, W.W., Crandall, P.H., Darcey, T.M., Becker, D.P., Levesque, M.F. and Barth, D.S. (1988), "The Magnetic and Electric Fields Agree with Intracranial Localizations of Somatosensory Cortex," Neurology, pp. 1705-14.

Weinburt, editor (1984), "Biomagnetism, Applications and Theory," Pergamon Press, New York.

Wikswo, J. P., Jr., Malmivuo, A. V., Barry, W. H., Leifer, M. C. and Fairbank, W. M. (1979), "The Theory and Application of Magnetocardiography," Advances in Cardiovascular Physiology, vol. 2, pp. 1-67.

Williamson, S. J. and Kaufman, L. (1978), "Application of SQUID Detectors in Biomagnetic Instrumentation," in NBS Special Publication 508, pp. 177-204.

Williamson, S. J. and Kaufman, L. (1984), "Frontiers in the New Science of Biomagnetism," Biomagnetism Applications and Theory, edited by H. Weinburg, G. Stroink, and T. Katila, Pergamon Press, pp. 471-90.

Williamson, S.J., editor, "Biomagnetism, an Interdisciplinary Approach," Plenum Press, New York, 1983